UNIVERSITY OF CALIFORNIA, SAN DIEGO

Recycling of Wasted Energy :

Thermal to Electrical Energy Conversion

A dissertation submitted in partial satisfaction of the

requirements for the degree Doctor of Philosophy

in

Materials Science and Engineering

by

Hyuck Lim

Committee in Charge:

Professor Yu Qiao, Chair
Professor Renkun Chen
Professor Shirley Meng
Professor Michael Todd
Professor Jie Xiang

2011

The dissertation of Hyuck Lim is approved, and it is acceptable in quality and form for publication on microfilm:

Chair

University of California, San Diego

2011

Dedicated to

my God and my family

" BE FAITHFUL EVEN TO THE POINT OF DEATH

AND

I WILL GIVE YOU THE CROWN OF LIFE.".

(Revelation 2:10)

TABLE OF CONTENTS

LIST OF FIGURES

LIST OF TABLES

ACKNOWLEDGEMENTS

First of all, I would like to express my sincere gratitude to my God.

I wish to acknowledge and deeply thank my advisors, Professor Yu Qiao for their strong encouragement, support, and direction during the course of this research. I wish to express my gratefulness to my committee members for their time and helpful suggestions: Professor Michael Todd, Professor Jie Xiang, Professor Shirley Meng and Professor Renkun chen.

I would also like to recognize and thank the following individuals for their assistance in various aspects of this work and my life: to Dr. Chulyoung Kim, my real friend and coworker for the Heaven's. Dr. Taewan Kim, Dr. Weiyi Lu and Brian Chow were always my friends and listeners about my life in the school and American society. Debra Bomar always understood the difficulties of the foreign students And Lindsay Walton may be the kindest person in the world. Without them, my school life would have been terrible in this different world. I want to thank you to Raquel Hall, because she opened the lab door whenever I had been locked out.

As this dissertation marks the important accomplishment in my life as a full time student and a researcher, I would also like to show appreciation to the following individuals who have taught, helped, and encouraged me along the way: Professor Shinhoo Kang in Korea, who is my uncle and made me start a scientist way, Professor Takashi Noguchi in Japan who showed me the true way as a researcher, Dr. Youngsoo Park who was my role model in Samsung, Dr. Seyoung Cho in HP who is a sincere senior in my life. They never avoid advising and helping me and my family. I cannot forget it.

Special thanks go to Charlotte Lauve for taking care of the administrative burdens for me.

I graciously acknowledge the financial support from DOE,NSF, San Diego city and Von Liebig Center.

I wish to thank my lovely wife, Jinhwa who sacrifice her life for me, my little Bit and Han, and finally my parents! I want to share this great joy with them forever.

I also wish to thank my all friends in La Jolla and other colleagues who are too numerous to mention all by name especially in Calvary Korean Church.

Hyuck Lim

La Jolla, August 2011

VITA

1976	Born in Seoul, South Korea
2000	B.S., Materials Science and Engineering, Seoul National University, Seoul, Korea
2002	M.S., Materials Science and Engineering, Seoul National University, Seoul, Korea
2011	Ph.D., Materials Science and Engineering, University of California, San Diego

SELECTED AWARDS

Awarded with the Materials Science Research Assistant Fellowship, University of California, San Diego for the year 2007-2011

Awarded with the travel fund from Korean-American Scientist and Engineers Association, for the year 2010.

Selected as Best Poster Presenters at IDW 2006

Awarded with the Dept of Materials Science and Engineering Fellowship, Seoul National University, Seoul, Korea for the year 1998.

PUBLICATIONS

Journals Articles:

1. " Thermal to electrical energy conversion" , Yu Qiao, V.K Punyamurtual, Aijie Han, **Hyuck Lim,** Journal of Power source 183, p403 (2008)

2. "Amorphous silicon thin-film negative electrode prepared by low pressure chem ical deposition for lithium ion batteries", Hunjoon Jung, Min Park, Shinhee Han , **Hyuck Lim** and SeungKi Joo, Solid state communications. Vol.125, pp 387 (2 003)

3. " Effects of surface charging treatment on outer and inner surfaces of a nanopor ous carbon", Weiyi Lu, Ajie Han, Taewan Kim, **Hyuck Lim**, Yu Qiao, J ournal of Materials Researches., Vol. 24, No. 8 (2009)

4. " Electrically controlled hydrophobicity in a surface modified nanoporous carbo n", Kim T, Lu W, **Lim H**, Han A, Qiao Y. Applied Physics Letters, Vol. 98, 05 3106.1-3 (2011)

5. " Ion repeling effect of nanopores in a hydrophobic zeolite", Brian Chow, Weiyi Lu, Aijie Han, **Hyuck Lim**, Yu qiao, Journal of Materials Researches, publishe d online (2011)

6. "Effects of Ion Concentration on Thermally-Chargeable Double-Layer Superca pacitors" **Hyuck Lim**, Yu Qiao, to be submitted

7. "Dependence on Cation Size of Thermally Induced Capacitive Effect of a Nano porous Carbon" **Hyuck Lim**, Yu Qiao, to be submitted

8. "Anion Size Effect on Zeta Potential in a Nanoporous Carbon" **Hyuck Lim**, Yu Qiao, to be submitted

9. "Thermal Sensitivity of Zeta Potentials of A Few Metallic Materials" **Hyuck Li m**, Yu Qiao, to be submitted

10. "Performance of Thermally-Chargeable Supercapacitors in Various Solvents" **H yuck Lim**, Yu Qiao, to be submitted

11. "Using Thermally-Chargeable Supercapacitor for Fluctuating Low-Grade Heat Sources" **Hyuck Lim**, Yu Qiao, to be submitted

12. "Double gate GaInZnO thin film transistors" **Hyuck Lim** et al. Journal of Materials Researches, Vol. 93, 063505 (2008)

13. Source/Drain Series-Resistance Effects in Amorphous Gallium–Indium Zinc-

Oxide Thin Film Transistors Jaechul Park, Changjung Kim, Sunil Kim, Ihun Song, Sangwook Kim, Donghun Kang, **Hyuck Lim**, Huaxiang Yin, Ranju Jung, Eunha Lee, Jaecheol Lee, Kee-Won Kwon, and Youngsoo Park, IEEE Electron Device Letters, Vol. 29, NO. 8, (2008)

14. "Program/Erase Characteristics of Amorphous Gallium Indium Zinc Oxide Nonvolatile MemoryHuaxiang Yin, Sunil Kim, **Hyuck Lim**, Yosep Min, Chang Jung Kim, Ihun Song, Jaechul Park, Sang-Wook Kim, Alexander Tikhonovsky, Jaewoong Hyun, and Youngsoo Park, IEEE Transactions on Electron Devices, Vol. 55(8) (2008)

15. "Amorphous gallium indium zinc oxide thin film transistors: Sensitive to oxygen molecules DongHun Kang, **Hyuck Lim**, ChangJung Kim, Ihun Song, Jaecheol Park and YoungSoo Park, Applied Physics Letters, Vol.90, p.192101 (2007)

16. "Ultra low sheet resistance on poly silicon film excimer laser activation", **Hyuck Lim** et al, Journal of the Korean Physics Society, Vol. 48, p s47 (2006)

17. "Ultra low temperature process by ion shower doping technique for polySi TFT on plastic", JongMan Kim, **Hyuck Lim**, DoYoung Kim, Ji-Sim Jung, JangYeon Kwon and Takashi Noguchi, Journal of the Korean Physics Society, Vol. 48, p s51(2006)

18. "A New approach of poly crystalline silicon film on plastic substrate prepared b y Ion Beam Deposition followed by excimer laser crystallization at room tempe -rature", JangYeon Kwon, **Hyuck Lim**, KyungBae Park, JiSim Jung, DoYoung Kim, Hans S. Cho, SeokPil Kim, YoungSoo Park, JongMan Kim and Takashi N oguchi, Japanese Journal of Applied Physics, Vol 45, No 5B, p 4362 (2006)

19. "Oxygen Effect on laser crystallization of sputtered a-Si Film on plastic substrate", DoYoung Kim, JongMan Kim, Ji-Sim Jung, JangYeon Kwon, Hans S. Cho, KyungBae Park, **Hyuck Lim** and Takashi Noguchi, Japanese Journal of Applied Physics Vol. 45, No. 3, p. L74 (2006)

20. "Advanced Poly-Si TFT with Fin like channels by ELA", Huaxing Yin, Wenxu Xianyu, JangYeon Kwon, Hans S. Cho, Xiaoxin Zhang, Ji-Sim Jung, DoYoung Kim, **Hyuck Lim**, KyungBae Park, JongMan Kim, and Takashi Noguchi, IEEE EDL Vol. 27, No. 5, p 357 (2006)

21. "Ultra low temperature poly-Si thin film transistor for plastic substrate", DoYou ng Kim, JangYeon Kwon, Ji-Sim Jung, KyungBae Park, Hans S. Cho, **Hyuck L im**, JongMan Kim, Huaxing Yin, Wenxu Xianyu and Takashi Noguchi, Journal of the Korean Physical Society, Vol. 48, p s61(2006)

22. “Low temperature process for adanced Si Thin film transistor technology”, Takashi Noguchi, JangYeon Kwon, Ji-Sim Jung, JongMan Kim, KyungBae Par k, **Hyuck Lim**, DoYoung Kim, Hans S. Cho, Huaxing Yin, Wenxu Xianyu, J apanese Journal of Applied Physics, Vol. 45. No. 5B, p4321 (2006)

23. “Amorphous silicon film deposition by low temperature catalytic chemical vapo r deposition and laser crystallization and poly-Silicon thin-film transistor applic ation”, SungHyun Lee, WanShick Hong, JongMan Kim, **Hyuck Lim**, KyungBa e Park, ChulLae Cho, KyungEun Lee, DoYoung Kim, JiSim Jung, JangYoen K won and Takashi Noguchi, Japanese Journal of Applied Physics, Vol. 45, No.8, p L227 (2006)

24. “Control of Carbon nanotube’s shape by ion bombardment” **Hyuck Lim**, Hunjo on Jung, SeungKi Joo, Microelectronic Engineering,Vol. 69, p81(2003)

25. “A New Process for removal of catalyst in Carbon Nanotube grown by hot fila ment chemical vapor deposition” **Hyuck Lim**, Hunjoon Jung, CheolHo Park an d SeungKi Joo, Japanese Journal of Applied Physics, Part 1, Vol. 4, p 4686 (200 2)

Patents / Technology disclosures:

1. 7439197 "Method of fabricating a capacitor"

2. 7470579 "Method of manufacturing a thin film transistor "

3. 7700954 "Transistor, method of fabricating the same and organic light emitting… "

4. 7629207 "Bottom gate thin film transistor and method of manufacturing the same… "

5. 7750424 "Microlens and an image sensor including a microlens “

6. 7662678 "Method of forming a more highly-oriented silicon layer and substrate having… "

7. 7859054 “ Poly-Si thin film transistor and organic light emitting display…”

Conference proceedings:

1. “Developing Advanced Thermoelectric and Mechanoelectric systems using nanoporous materials” **Hyuck Lim**, Alice Han and Yu Qiao, Earth & Space 2008 Conference (Long Beach, USA)

2. “Study of Ulatra low resistance n-type and p-type poly-Si Film”, **Hyuck Lim** et al., IMID 05(Korea)

3. “The fabrication of the p-type Ultra low temperature TFT under 200^{o}C”, **Hyuck Lim** et al , IDW 2005(Japan)

4. “Study of junction offset by using tilted dopant implantation method”, **Hyuck Li m** et al, ITC 2006(Japan)

5. “2.2 inch qqVGA AMOLED dried by ultra low temperature poly-Si TFT direct f abricated below 200^{o}C”, JangYeon Kwon, Ji-Sim Jung, KyungBae Park, JongM an Kim, **Hyuck Lim**, Takashi Noguchi and JongMin Kim, SID 2006(USA)

6. “Selective epitaxy for 3D LSI”, Hans S. Cho, Wenxyu Xianyu, Hua Xian Yin, H yuck Lim and Takashi Noguchi, ISDRS 2005 (USA)

7. “Highly (100) oriented Si Thin films onto insulator substrates using ultra-thin-Al 2O3 by oxidized (002) AlN buffer layer γ”, Wenxu Xianyu, **Hyuck Lim**, Huaxi ng Yin, Hans S. Cho, JoonHo Lee, YoungNam Kwon, JungHyun Lee and Youn gsoo Park, 2006 MRS fall (USA).

8. “Effect of ion damage on the shape of carbon nanotube”, **Lim Hyuk**, Hunjoon Jung, ByoungDong Kim, WonSick Shin, ChoelHo Park, 2001 MRS fall (USA)

ABSTRACT OF THE DISSERTATION

Recycling of Wasted Energy :

Thermal to Electrical Energy Conversion

by

Hyuck Lim

Doctor of Philosophy in Materials Science and Engineering

University of California, San Diego, 2011

Professor Yu Qiao, Chair

Harvesting useful electric energy from ambient thermal gradients and/or temperature fluctuations is immensely important. For many years, a number of direct and indirect thermal-to-electrical energy conversion technologies have been developed. Typically, direct energy conversion is achieved by using thermoelectric generators or thermogalvanic cells; indirect energy conversion is achieved by using Organic Rankine Cycle or Sterling Engines.

On the one hand, there is a fundamental technical difficulty, thermal shorting, that limits the energy conversion efficiency of direct thermoelectric energy conversion methods. While extensive study has been conducted in this area, currently the portion of thermal energy that can be converted to electricity is still small. On the other hand, the indirect energy conversion systems tend to be complicated and expensive. Thus,

existing energy harvesting technologies are less economically competitive compared with the grid power.

To develop advanced energy harvesting systems, a novel concept using nanoporous materials is investigated. Nanoporous materials have been widely used as advanced absorbents. Because of their ultra-large surface areas (100-2000 m^2/g), they can adsorb a large amount of ions when they are immersed in electrolyte solutions. The ion adsorption capacity is thermally dependent. If two nanoporous electrodes are placed at different temperatures, they adsorb different amounts of ions, generating a net output voltage. The thermally driven ion motion causes a transient current, which can be reactivated through temperature fluctuation or internal grounding. The two electrodes are isolated; that is, the direct heat loss between them is minimized. Our experimental data have shown encouraging results: the output voltage and the energy conversion efficiency are higher than that of conventional thermoelectric materials by orders of magnitude.

Our study will not only lead to the development of high-performance thermal energy harvesting systems, but also shed light on fundamentals of electrophysics in nanoenvironment. The thermal effect on surface electrification (i.e. the capacitive effect) in nanopores is a new scientific area. Conventional interface theories have failed in explaining a number of experimental observations. We have carried out a systematic study of the effects of ions, solvent, electrode, cell configuration, etc. to understand the fundamental mechanisms and processes that govern the ion motion and charge transfer in nanopores.

CHAPTER 1. Introduction

1.1. Low Grade Heat (LGH) is ample

Low Grade Heat (LGH) is often referred to as the thermal energy from low-temperature heat sources below 250^{o}C. In the U.S. alone, many Giga Watt of energy is wasted as LGH. For example, in solar farms, ~80% of solar energy is eventually wasted as LGH; and in a vehicle, 60% of the chemical energy is wasted as LGH.

Harvesting and storing LGH is still a blank area of today's technology [1]. In such a low temperature range, many technologies that work well at higher temperatures become economically and/or energetically inefficient. For instance, most of direct heat storage methods based on phase transformation or chemical reactions are irrelevant for LGH [2]. A few available LGH storage materials, e.g. paraffin [3], are too expensive for large-scale systems. An intrinsic difficulty is associated with the low thermal energy density of LGH. One possible solution is to harvest, convert, and store LGH in other forms, e.g. electric energy, by employing systems of higher energy densities. Converting LGH to electric energy also helps transport and directly utilize the harvested and stored energy. In the next section, we will discuss the conventional technologies such as Organic Rankine Cycle (ORC) mahines, Sterling engines, and thermoelectric energy generation (TEG)

1.2. Conventional Energy Conversion Technologies

1.2.1. Direct energy conversion

In a direct energy conversion system, heat can be converted into electricity through spontaneous thermally related phenomena, e.g. in a thermoelectric generator or a thermogalvanic (TG) cell [4]. With two dissimilar conductors, when each junction of the two is at different temperature, electromotive force (ϕ) is developed between the junctions.

1.2.1.1. Thermoelectric Generator

In a thermoelectric generator (TEG), the key component is the thermoelectric material. The advanced thermoelectric materials include: (1) superlattices consisting of periodic thin layers of different materials [5], in which the heat conductivity is reduced while the electron transport is enhanced, due to phonon/electron scattering and band structure modification at layer interfaces; (2) nanowires/nanotubes [6], in which the electron density of states at the Fermi level is increased, due to quantum size effect; and (3) complex oxides of low thermal conductivity and high electric conductivity [7]. Their energy conversion efficiency is often measured by the dimensionless figure of merit $Z = \alpha^2/\kappa\lambda$, where $\alpha = \phi/\Delta T$ is the temperature sensitivity of output voltage, also known as the Seebeck coefficient, with ϕ and ΔT being the output voltage and the temperature difference, respectively; κ is the electric resistivity; and λ is the thermal conductivity. For conventional thermoelectric materials, the values of figures of merit are below 0.1, and therefore their applications are mostly limited to temperature measurement. Recently, enhanced figures of merit around 2-5 were achieved [8]. The energy conversion efficiency can also be directly calculated as $\zeta = \zeta_c \cdot \zeta_Z$, where $\zeta = U_e/U_t$, with

U_e and U_t being the generated electric energy and the consumed thermal energy, respectively; ζ_c is the Carnot cycle efficiency; and ζ_Z is a function of Z ($\frac{\sqrt{1+ZT}-1}{\sqrt{1+ZT}+\frac{T_C}{T_H}}$ where T_C and T_H are temperatures at cold and hot ends, respectively), typically smaller than 10%.

1.2.1.2. Thermogalvanic cell

If a temperature gradient exists in electrolyte solution, it leads to a gradient in the chemical potential in it, which depends on the magnitude of the heats of transport of a given ion. The heat of transport is the energy required to transport the ion between regions of different temperature. [9] This is called as Soret effect. The performance of many kinds of thermogalvanic cells are listed in Table I. [10,11] The power conversion efficiency is formulated as $V^2_{OC}/(4R\kappa A\cdot(\partial T/\partial x))$, where VOC is the open circuit potential between the electrodes, R, κ, A, and $\partial T/\partial x$ are cell resistance, thermal conductivity, the cross-sectional area of the ion path, and temperature gradient. [12] To enhance the conversion efficiency, the temperature sensitivity should be high and internal resistance and thermal conduction should be reduced. The temperature sensitivity can be representative by Seebeck coefficient, which is depending on materials' properties. In the table, the maximum Seebeck coefficient is -4.17 mV/K. This number is much higher compared to numbers of solid state thermoelectric materials, which has around a few hundred μV/K.[1] However, the conversion efficiency is less than one and the ratio to Carnot efficiency is only 1.5. This is because other factors such as internal resistance and thermal conductance are too high. The

reason of the high cell resistance is due to the distance between the electrodes. If they are close to each other, the thermal conductance should be very large. There have been many trials to reduce the two factors by changing the cell configuration [13,14], however, the innate problem is still pulling over the technology.

Table 1.1. Summary of the various thermogalvanic cells

solvent	cell description	Seebeck coefficient (mV/K)	Power conversion Efficiency (%)	Ratio to Carnot effi. (%)
H_2O	Pt// 2M Fe^{2+}/Fe^{3+}, 1M HCl//Pt	0.57	0.005	0.035
	Pt// 0.2M $Fe(CN)_6^{3-}/Fe(CN)_6^{4-}$, 0.5M K_2SO_4 //Pt	1.4	0.047	0.33
	Pt// 1M $(NH_4)_4Fe(CN)_6$, 2M NH_4Cl //Pt	2.9	0.2	1.2
	Cu// 0.35M $Cu(HCOO)_2$, 0.35M $NaHCO_3$ //Cu	1.2	0.03	0.2
	Pt// 0.07M $Fe(CN)_6^{3-}/Fe(CN)_6^{4-}$, 3M KCl //Pt	1.6	0.028	0.44
	Pt// 0.26M $Fe(CN)_6^{3-}$/0.26M $Fe(CN)_6^{4-}$, 0.8M KCl//Pt	1.5	0.031	0.5
	Cu// $CuSO_4$ 20wt% //Cu	1.45	0.023	0.1
	Pt// $xK_4Fe(CN)_6$, $yK_3Fe(CN)_6$, zKCl //Pt	-1.8	0.3	1.5
	Cu// $xCuTAAB(NO_3)_3$, $yCu(TAAB(NO_3)$, zKCl //Pt	-1.86	0.34	1.7
	Cu// $xCu(fen)_2Cl_2$, $yCu(fen)_2Cl$, zKCl //Cu	-1.84	0.33	1.6
	Cu// $xCu(dipy)_2Cl_2$, $yCu(dipy)_2Cl$, zKCl //Cu	-2.5	0.3	2.6
Butyrolactone	Cu// $zCu(dipy)_2Cl_2$, $jCu(dipy)_2Cl$, 1M $LiBF_4$ //Cu	-4.17	0.78	1.5
Molten salt	Ag// AgI(S) //Ag	-0.6	2.1	4.5
	Glassy Carbon// La, $LaCl_3$, LiCl-KCl //Glassy Carbon	-1.2	9.6	15.4
	SC// $BiCl_3$ in $AlCl_3$-NaCl-KCl //SC	2.25	6.27	17.8

1.2.2. Indirect energy conversion system

The working process of an indirect energy conversion system consists of multiple steps to convert thermal energy to electrical energy. Usually, heat is first converted to kinetic energy through phase transformation, and then converted to electrical energy by turbine engines. Organic Rankine Cycle (ORC) system or Sterling Engine (SE) are commonly used indirect energy conversion systems.

1.2.2.1. Organic Rankine Cycle system

For recovering LGH, an organic Rankine cycle (ORC) system generates electricity by forming gas steam using wasted heat and rotating turbine engines. Figure 1.1 is a schematic of the basic structure of ORC system. The fluid is evaporated in the evaporator and the gas stream rotates the turbine engine. The gas stream is condensed to liquid and then it is fed into the evaporator by a pump. In an ideal working cycle, the expansion is isentropic and the evaporation and condensation processes are isobaric. In reality, the presence of irreversible processes lowers the overall efficiency. By employing working fluid with different thermophysical properties, the working condition, e.g. the working temperature range, can be adjusted. Organic liquids, such as benzene, toluene, or p-xylene, are suitable to LGH applications. [15] Unlike water, most organic fluids suffer chemical decomposition and degradation at high temperatures/pressures. Most organic fluids have relatively low critical pressures and much smaller heat capacities than water. Therefore, an ORC system must be operated in the appropriate ranges of temperature and pressure. ORC systems have been utilized to

harvest LGH from the wasted heat in the condensers of power plants, the solar radiation, and the geothermal energy. [16]

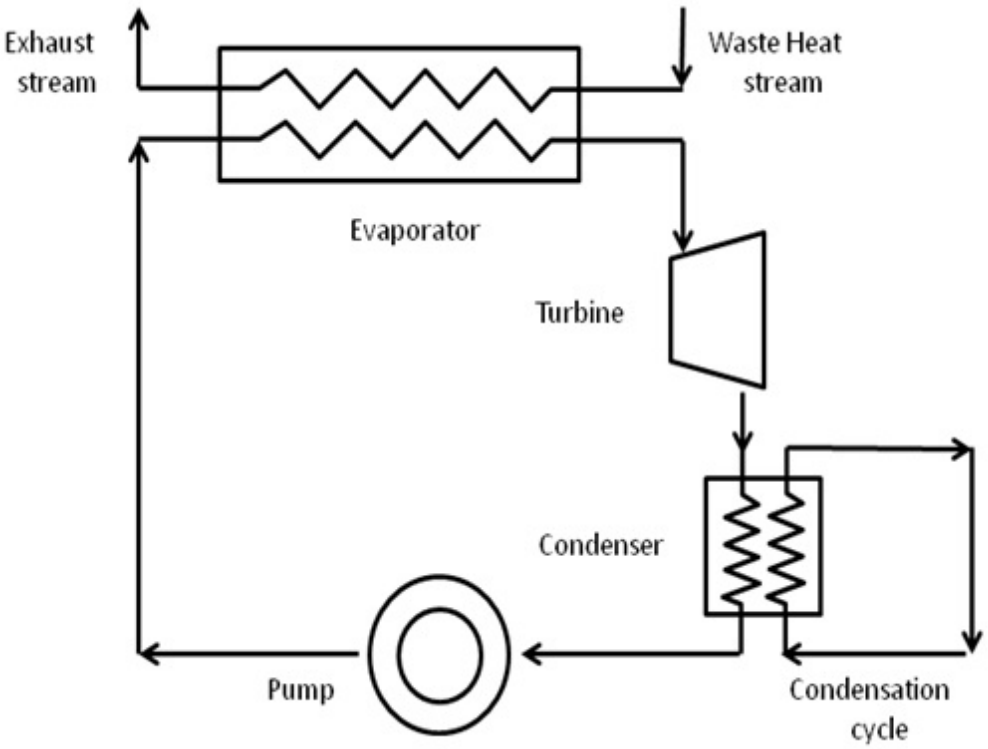

Fig. 1.1. Schematic of the Organic Rankine Cycle

1.2.2.2. Sterling engine

Sterling engine is a closed combustion system. Its working mechanism is based on the Sterling cycle, which involves expansion and contraction of a working gas, such as air, helium, or hydrogen, caused by an external heat source/sink. A Stirling cycle consists of two isothermal processes and two constant volume processes. In Fig.1.2, Segment 1-2 and Segment 3-4 are isothermal processes and Segment 2-3 and Segment 4-1 are isochoric processes. The ideal efficiency is the same with the Carnot efficiency, higher than that of other indirect energy conversion systems. In Fig.1.2, the regenerator carries out the internal heat exchange process. During heat exchange, the fluid repeatedly passes through the regenerator in opposite directions. The efficiency of the heat exchange is critical to the overall efficiency. The heat source can be solar thermal energy, biological thermal energy, geothermal energy, wasted heat from a nuclear reactor, etc. The heat sink can be constructed by using cold water or cold air. Currently, various types of Stirling engine have been developed, which are summarized in Table 1.2

Table 1.2. Table of summary of Sterling engine [17]

year	inventor	Feature
1816	Robert Stirling	100W ~ 4kW
1853	John Ericsson	220kW at 9rpm for a ship
1954	Philips lab	36~38% efficiency at 977K, 30~336kW
1978	Gupta	solar powered, compact type, 1~2kW, 5.5~5.7%
1989	Nakajima	Extremely small enegine (10g), 10mW
1999	Podesser	Biomass engine, 3.2kW, 25%
1999	Hoshino	Piston free, 30%
present	United stirling etc.	use sun-beam concentrator, over 40% at 973K, 200bar

(a)

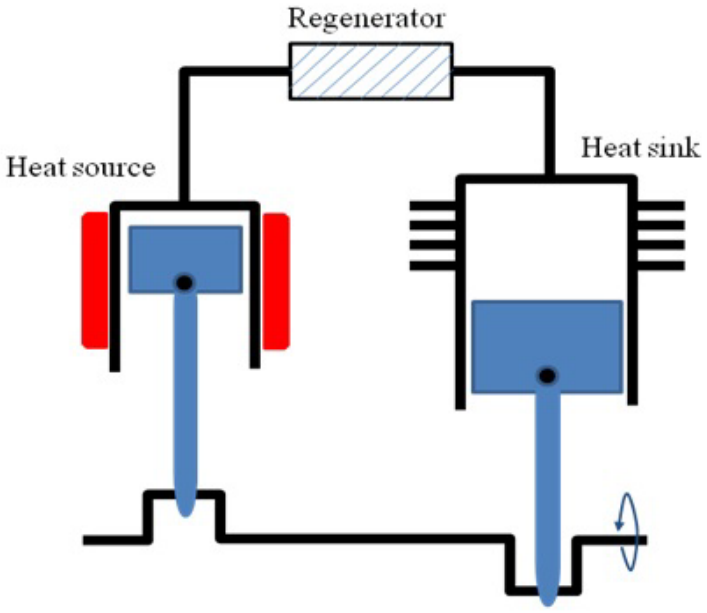

(b)

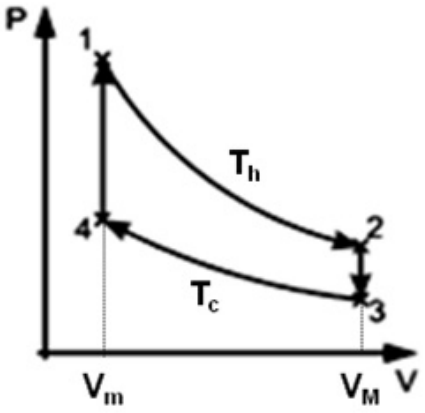

Fig.1.2. (a) Schematic of Sterling engine (b) P-V plot of the Sterling cycle

1.3. Cost-effectiveness of the conventional technologies

To commercialize the technologies to regenerate the low grade heat, cost analysis should be preceded. Based on existing literatures, we compared their cost-effectiveness as in the table I.3. In the temperature range from 30^{o}C to 70^{o}C, they were \$16/W, \$5.14/W, \$11/W, and \$3/W for TEG, thermogalvanic cell, SE, and ORC, respectively. Among them, the ORC shows the best cost-effectiveness, however, it is still too expensive to compete with conventional internal combustion engine (\$0.5/W). This is mainly because the ORC is bulky and needs complicate mechanical compartments; therefore the maintenance with high cost is inevitable. The second best one should be thermogalvanic cell. According to Renchong Hu's [18] cost analysis of their cell, the cost is calculated as \$5.14/W. Their using carbon material seems to make the cost saving. He expected that they could lower the cost if they were mass-produced.

Conclusively, we feel the need to create brand-new concept to realize highly efficient and practical LGH renerative system. In the next section, we will discuss the basic concept of our Nanoporous Thermal-to-electrical Energy Conversion System (NTEECS).

Table 1.3. Comparison of cost-effectiveness of several LGH regenerative systems.

	Cost per Watt (delta T 30C to 70C)	**Current Market Size (\$)**
TEG	~\$16/W	<\$1m
Thermogalvanic cell	~\$5.14/W	N/A
Stirling Engine	~\$11/W	~\$10m
ORC	~\$3/W	~\$50m
Internal Combustion Engine or Turbine (delta T 30C to 350C)	~\$0.50/W	~\$100,000m

1.4. Basic working principle of Nanoporous Thermal-to-electrical Energy Conversion System (NTEECS)

The NTEEC system, sometimes referred to as thermally chargeable supercapacitors (TCS), was recently developed in our lab [19]. It is based on the capacitive effects.

1.4.1. Electrical Double Layer

In a bulk electrolyte solution, anions and cations are uniformly distributed. If a solid material is immersed into the electrolyte solution, the ion distribution would become anisotropic in at the solid-liquid interface. In the interface zone, the solvated ions are subjected to different force fields from the solid and the liquid phases, resulting in different configurations of solvent dipoles and charged species. Once the electrolyte side of the interface has excess charges, a net electric field would be generated across the interface, and counter charges would be induced at the electrode side, leading to a potential difference. Because the thickness of the interface zone is typically quite small (0.1 to 1 nm), the field strength can be enormous, on the scale of 10^7 V/cm. The term "electrical double layer" is often used to describe the structure of the charges and the oriented dipoles constituting the solid-liquid interface region [20]

1.4.2. Ion density change in the Electrical Double layer

In an electrical double layer, the effective surface ion density is sensitive to the temperature change (Fig.1.3). According to the Poisson's equation, the relationship

between the excess ion density (ρ_r) in a representative volume element (RVE) and the electrostatic potential (Ψ_r) can be stated as: [20]

$$\frac{1}{r^2}\frac{d}{dr}\left(r^2\frac{d\psi_r}{dr}\right) = -\frac{4\pi}{\varepsilon}\rho_r \qquad \text{(Eq. 1-1)}$$

where r and ε are the distance from the arbitrarily selected central ion and the dielectric constant of the solution, respectively. In the solution, there are many types of ions. Denote n_i as the number of type i ions per RVE, and the corresponding ion charge is $z_i e_0$ (z_i is the valence of the ion and e_0 is the electronic charge). The excess charge density is [20]

$$\rho_r = \sum n_i z_i e_0 \qquad \text{(Eq. 1-2)}$$

According to the classic Boltzmann distribution law, [20]

$$n_i = n_i^0 e^{-U/(kT)} \qquad \text{(Eq. 1-3)}$$

where U is potential energy between ions; that is

$$U = z_i e_0 \psi_r \qquad \text{(Eq. 1-4)}$$

Combination of the above three equations gives [20]

$$\rho_r = \sum n_i z_i e_0 = \sum n_i^0 z_i e_0 e^{\frac{z_i e_0 \psi_r}{kT}} \qquad \text{(Eq. 1-5)}$$

where n_i^0 is the bulk concentration. The equation can be linearized by using Taylor series under the condition that electrostatic potential (ψ_r) is much smaller than the thermal energy (kT): [20]

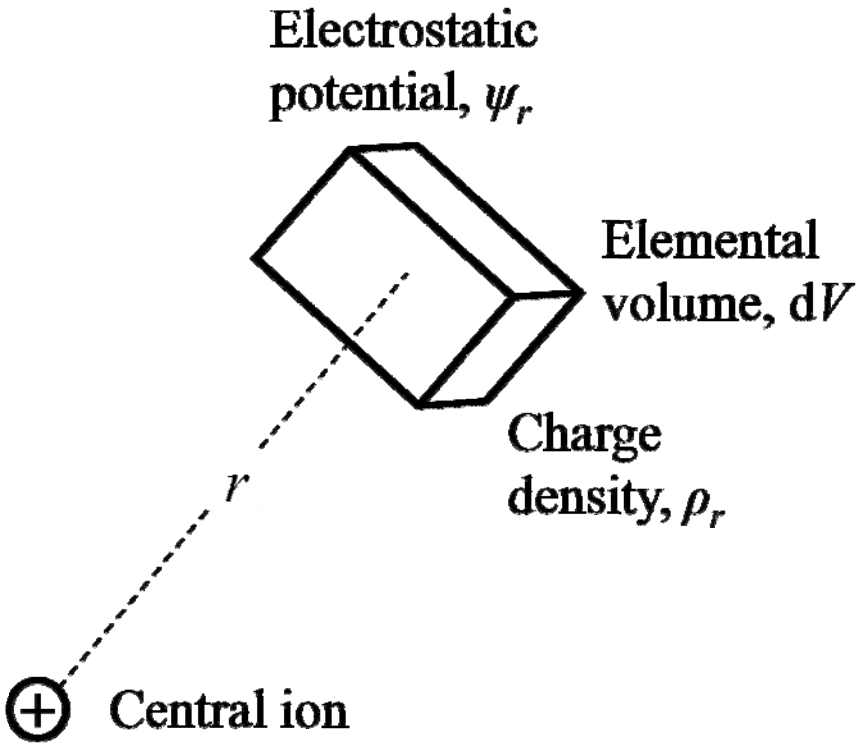

Fig.1.3. Charge density of elemental volume located from a central ion at a distance *r*

$$\rho_r = -\sum \frac{n_i^0 z_i^2 e_0^2 \psi_r}{kT} \quad \text{(Eq. 1-6)}$$

Finally, the linearized Poisson-Bolzman equation can be obtained by relating the Poisson equation to the linearized Boltzmann equation: [20]

$$\frac{1}{r^2}\frac{d}{dr}\left(r^2 \frac{d\psi_r}{dr}\right) = \kappa^2 \psi_r \quad , \quad \kappa^2 = \frac{4\pi}{\varepsilon kT} \sum n_i^0 z_i^2 e_0^2 \quad \text{(Eq.1-7)}$$

This equation is for a single central ion. It can be applied to any electrode immersed in an electrolyte solution. The major difference is the geometry: the central ion is spherical; a large electrode surface is planar.

Because the Fermi energy of electrode material is different from that of the electrolyte solution, there are electrostatic forces between the electrode and the ions. To analyze the relationship between the electric field and the potential *x* away from the electrode, a few models were developed, such as the Helmholtz-Perrin parallel plate model, the Gouy-Chapman model, and the Stern model, which is a combination of the former two models.

According to the Gouy-Chapman's model,[20]

$$\frac{d\psi}{dx} = -\left(\frac{8kTc_0}{\varepsilon\varepsilon_0}\right)^{\frac{1}{2}} sinh\frac{ze_0\psi_x}{2kT} \quad \text{(Eq. 1-8)}$$

where c_0 is the concentration of the ions in the bulk solution, ε is the dielectric constant of the solution, ε_0 is the permittivity of free space, and ψ_x is the outer potential difference between a point *x* away from the electrode and the bulk solution. Following

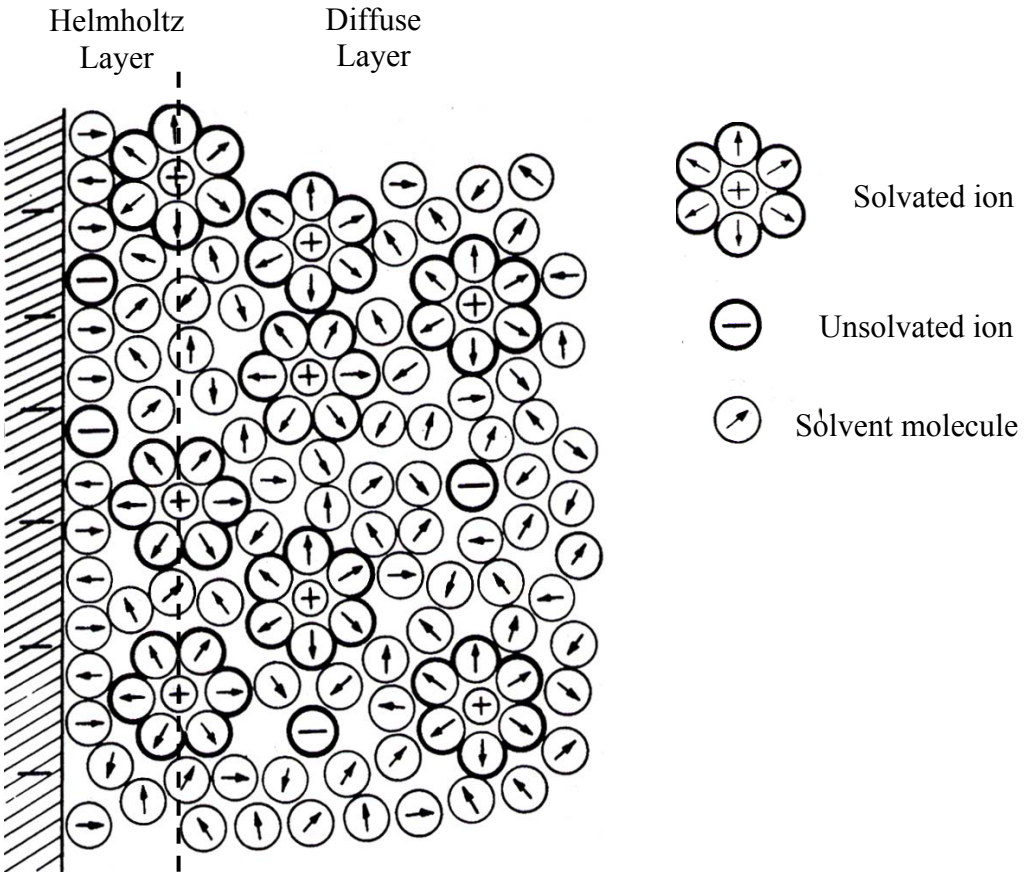

Fig.1.4**.** Schematic of double-layer structure of solvated ions at a solid surface The solid surface absorbs ions and the interface is electrified spontaneously. [19]

the Gaussian law, we can calculate the amount of the charges in the diffusion layer (q_d): [20]

$$q_d = -2(2\varepsilon\varepsilon_0 c_0 kT)^{\frac{1}{2}} \sinh\left(\frac{ze_0\psi_0}{2kT}\right) \quad \text{(Eq. 1-9)}$$

where ψ_0 is the potential at $x = 0$, with respect to the bulk solution phase.

The capacity of the layer is [20]

$$C_G = \left(\frac{2\varepsilon\varepsilon_0 z^2 e_0^2 C_0}{kT}\right)^{\frac{1}{2}} \cdot \cosh\frac{ze_0\psi_M}{2kT} \quad \text{(Eq. 1-10)}$$

Based on the Gouy-Chapman model, Stern suggested that the ions in the interface layer and distributed in the thermal disarrays must be taken into consideration, which gives another capacitance component (C_H). Thus, the total capacitance should be [20]

$$\frac{1}{C} = \frac{1}{C_G} + \frac{1}{C_H} \quad \text{(Eq. 1-11)}$$

The electrical double layer is depicted in Fig.1.4.

1.4.1 Nanoporous electrode : High surface area

Nanoporous material is a kind of nanovoid-surrounding network, which is usually covalently bonded together [21]. Diatoms and abalone shells are well-known examples of a variety of nanoporous organic-inorganic hybrids in nature. [22]. Over tens of years, Synthetic methods for a large number of nanoporous materials have been in the middle of the materials science. Among them, the templating technique is one of the most well-known techniques, in which the template ranged from nano to micro size is formed first by phase separation or nanocasting, and then the template is removed by burning or etching [23-25]. A synthetic nanoporous material can be either of an ordered or disordered porous structure, with the high effective surface area. It is typically 100-2000 m^2/g, 6-8 orders of magnitude larger than in a bulk phase [26].

Zeolites and nanoporous carbons are the well-developed microporous materials (the nanopore size $2r < 2$ nm). There are more than 100 different kinds of natural or synthetic zeolites or zeolite-like materials, most of which can be used as molecular sieves that pass only molecules smaller than their pore sizes [27]. As for the nanoporous carbons, there are carbon blacks and activated carbons, which can be synthesized by various physical or chemical treatments of organic precursors or graphite [28-30] (as in Fig.1.5). They can be applied as battery electrodes, separation filters, substrates for catalysts, etc. CNT is another important material, which has been a subject of active research since Ijima found it [31]. Silica is one of the most widely used materials for mesoporous processing (2 nm $< 2r <$ 50 nm) as a template. Synthesis techniques for

(a)

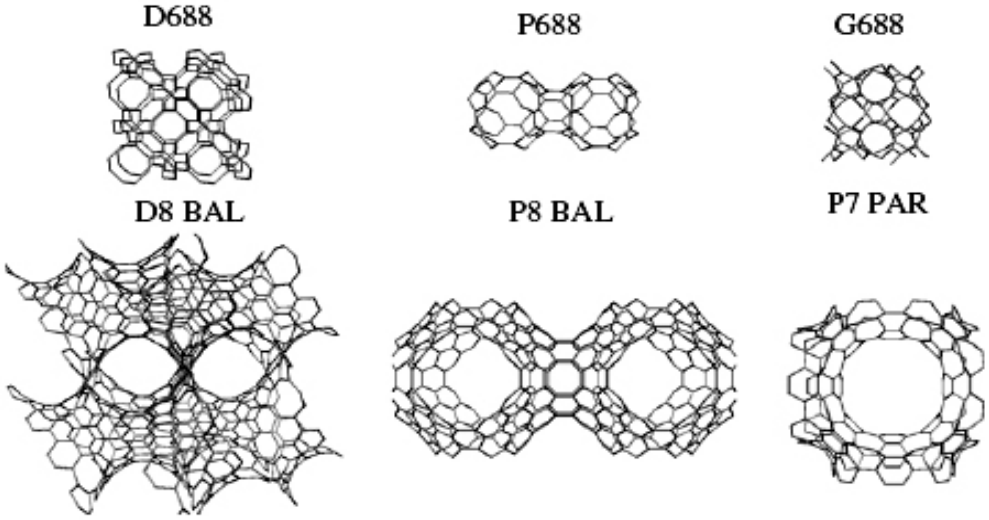

(b)

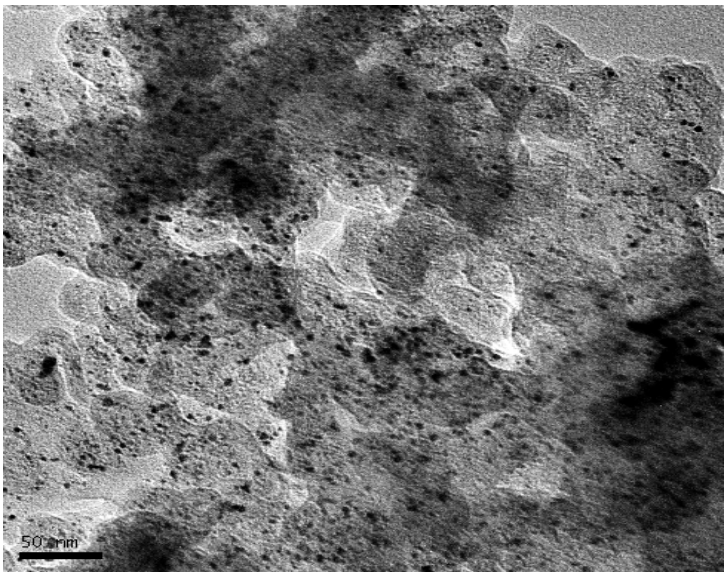

Fig.1.5. (a) Atomic structures of a few nanoporous carbons [31]; (b) TEM photo of a nanoporous carbon studied in the preliminary test.

silicas have been so established that various pore sizes, pore shapes, pore volume fractions, and surface structures are controllable [32]. They have been applicable to various types of applications covering sensing, catalysis, and molecular sieve. In addition, phosphates, transition metal oxides, and alumina can also be used to synthesize mesoporous materials [33]. For macroporous processing ($2r$ > 50 nm), metals, polymers, alumina, etc. are suitable candidates as templates.

In summary, a variety of nanoporous materials and their processing technologies have been developed. The overall pore structures can be controlled with precision. Additionally, a number of surface functionalizations and doping techniques have been developed adjusting nanopore surface characteristics such as conductive, semiconductive or insulating. Conductive or semiconductive nanoporous materials include carbons, titanium oxide, alkali metal doped zeolites, and metal alloys of copper or gold [34,35].

1.4.2 Working principle : Capacitive effect

The surface ion distribution at a solid-liquid interface is field responsive [36-40]. For instance, when a voltage is applied across the interface, the energy well confining ion motion in electric double layer (EDL) becomes deeper, and thus the interface ion density increases, so does the change in electrode potential ($\Delta\phi$). The increase in total amount of interface charges can be estimated as the excess ion density multiplied by the total surface area, $\Omega^* = \sigma_M \cdot A$. Thus, if the area, A, is large, this system can be of a large capacity. Based on this concept, double-layer supercapacitors have been developed by

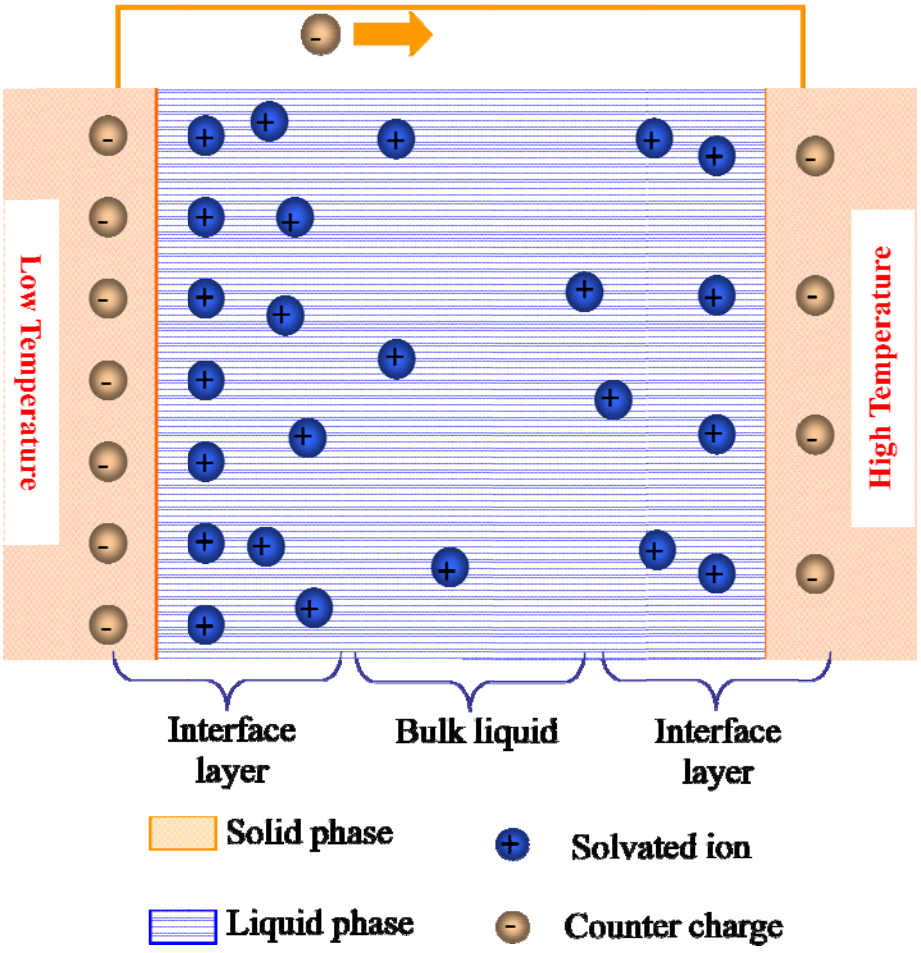

Fig.1.6. Schematic of two identical solid-liquid interfaces at different temperatures.

using nanoporous materials that have specific surface areas around 500-1500 m^2/g [41-43], and have been productized to power electric shuttle buses [44].

It is well known that the surface ion density (σ_M) is also thermally dependent [20]. As temperature increases, because the ions become more mobile, it becomes easier for them to overcome the energy well and move away from the interface. Thus, both σ_M and $\Delta\phi$ decrease [45]. The energy density of a double-layer capacitor can be reduced by more than 25% as temperature changes by 30-40 ^oC [46]. In the past, this energy "loss" was usually regarded as a detrimental factor.

Consider two identical solid-liquid interfaces, as depicted in Fig.1.6. Their temperatures are different. At the higher temperature, the interface ion density and potential difference are lower. Therefore, when the two interfaces form a circuit, excess charges would move from the low-temperature (high-potential) end to the high-temperature (low-potential) end, until the new equilibrium is established. The generated transient electric energy is converted from thermal energy. The total amount of generated charges (the charges that can move between the two interfaces) can be estimated by Eq.(I-9). Clearly, to enhance the system performance, the surface area, A, must be maximized. Similar to the double-layer supercapacitor, the electrode should be nanoporous. Moreover, for ordinary electrode materials, the thermal sensitivity of surface ion density is relatively low. To increase the energy conversion efficiency, the pore surface properties should be modified. From the next chapters, we will discuss the governing factors for the high energy conversion efficiency, and in the last chapter, we will report how much energy could be generated from the thermal energy in our NTEEC system.

CHAPTER 2. Effects of Ion Concentration on Thermally-Chargeable Double-Layer Supercapacitors

2.1. Introduction

While harvesting, storage, and utilization of thermal energy has been an active research topic for centuries [e.g. 47,48], low-grade heat (LGH), thermal energy associated with low-temperature heat sources with temperature (T) lower than 250 ^{o}C, is still a blank area of today's technology [49]. In such a low temperature range, many technologies that work well at higher temperatures become economically and/or technologically inefficient. For instance, most of direct heat storage methods based on phase transformation or chemical reactions are irrelevant for LGH [50]. A few available LGH storage materials, e.g. paraffin [51], are too expensive for large-scale systems.

An intrinsic difficulty is associated with the low thermal energy density of LGH. One possible solution is to harvest, convert, and store LGH in other forms, e.g. electric energy, by employing systems of high energy densities. Converting LGH to electric energy also helps transport and directly utilizes the harvested and stored energy.

However, conventional thermal-to-electric energy conversion (TEEC) techniques work poorly in the temperature range of LGH. A TEEC system typically works in between a high-temperature heat source and a low-temperature heat sink. Its energetic efficiency can be calculated as $\zeta = \zeta_c \cdot \zeta_s$, where $\zeta_c = \Delta T/T_h$ is the Carnot cycle limit and ζ_s is the system efficiency, with $\Delta T = T_h - T_l$ and T_h and T_l the temperatures of the heat source and the heat sink, respectively. As ΔT of LGH is small, the Carnot cycle

limit becomes low and, thus, the system efficiency must be ultrahigh to achieve an acceptable overall efficiency.

Indirect TEEC techniques, such as Organic Rankin Cycle (ORC) machines and turbine engines, do not meet this requirement. They are often used for applications where $\Delta T > 350\ ^{o}C$ [52], e.g. in coal power plants and concentrated solar thermal energy farms. They demand bulky, massive, and expensive components such as heat exchangers and pumps. The numerous moving parts also increase the installation, operational, and maintenance costs. Direct TEEC technology is often achieved by using thermoelectric materials, which, again, due to the low value of ζ_s in the LGH range, cannot be widely applied in engineering practice.

Note that the Seebeck effect, the working mechanism of thermoelectric materials, is not the only phenomenon provided by nature that is both thermally and electrically related. Many other phenomena, e.g. the thermally induced capacitive effect to be discussed in this paper, also involve energy conversion between heat and electricity. While in the past they were regarded as trivial, with the development of novel materials and energy techniques, these concepts should be re-investigated.

Consider two identical supercapacitor-type devices, as depicted in Fig.2.1(a). Each cell is a half-supercapacitor, consisting of a nanoporous electrode immersed in an electrolyte solution. Figure 2.1 (b) shows a double-layer (DL) supercapacitor. As a voltage is applied across the anode and the cathode, ions would be adsorbed at the electrode surfaces, and electric energy is stored as surface charges. Usually, the electrodes are nanoporous, so that the specific surface areas, A, are ultrahigh ($\sim 10^3\ m^2$ per gram of electrode). The large value of A greatly amplifies the system capacitance.

Depending on the liquid and electrode materials, the working voltage ranges from a fraction of to a few volts [53].

The high-ion-density surface layer can be formed spontaneously at the electrode-liquid interface, even without the external voltage [54]. The excess surface ions induce surface charges in the electrode phase, leading to the formation of electrode potential (ϕ). The electrode potential is thermally dependent: When temperature varies, as the mobility of surface ions is changed, the surface ion density becomes different, so does ϕ. Therefore, the two electrodes in Fig.2.1(a) are of different potentials. When they are connected, charges would move from the high-potential end to the low-potential end, converting the absorbed thermal energy to electric energy. This capacitive process is fundamentally different from the Seebeck effect, as the charge motion and the thermal conduction are separated. Hence, thermal shorting, which causes the low energetic efficiency of thermoelectric materials, can be prevented. Due to the presence of the liquid phase, such a system may not work at a high temperature, but can have a high performance in the LGH range, as the thermal sensitivity of electrode potential can be much higher than the Seebeck coefficients of thermoelectric materials. It will be referred to as thermally-chargeable supercapacitors (TCS) in the following discussion.

2.2. Experimental

To validate the feasibility of TCS for LGH, we investigated a nanoporous carbon (Cabot BP2000). The as-received material was in powder form. By using a Micromeritics ASAP2000 Analyzer, a gas absorption analysis was performed and the

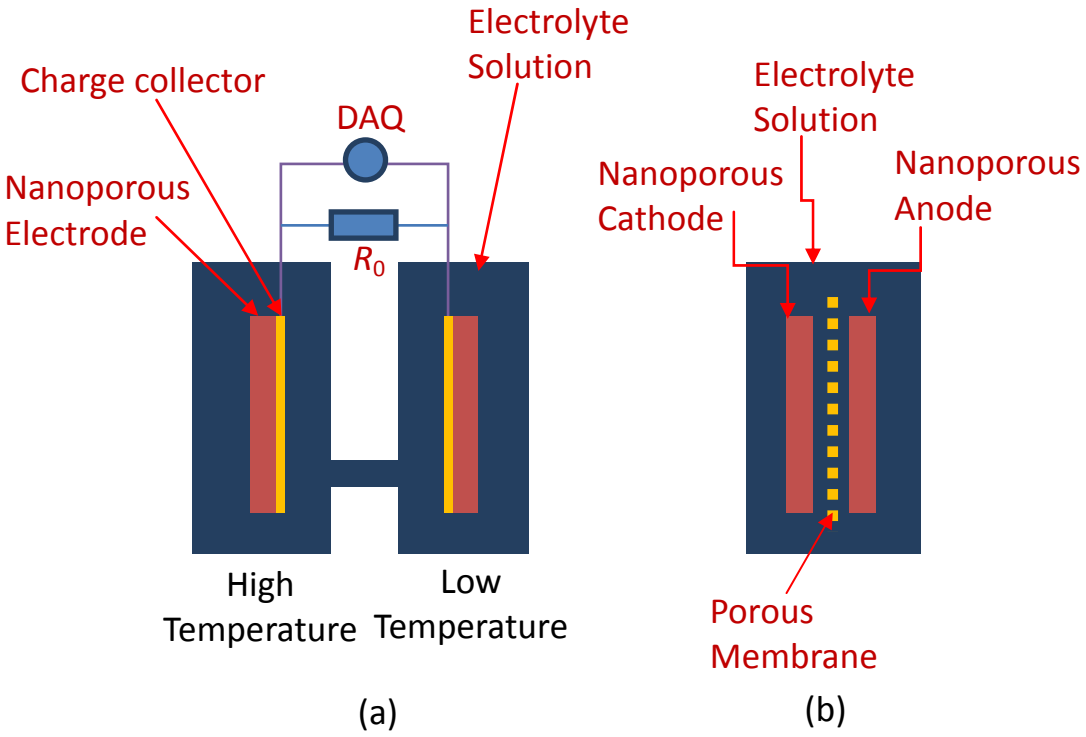

Fig.2.1. Schematics of (a) a thermally-chargeable supercapacitor (TCS) and (b) a double-layer (DL) supercapacitor.

range of nanopore size distribution was determined as 2 to 100 nm, with the modal value at 3 nm. The specific surface area was about 1800 m^2/g. It was refluxed in acetone for 4 hours, and then dried in vacuum at 80 ^oC for 10 h. In a stainless steel mold, the refluxed carbon powders were compressed at 400 MPa for 5 min, so as to form electrode disks. The mass of each disk is around 100 mg.

Two identical nanoporous carbon (NC) disks were firmly pressed on platinum (Pt) sheets and soaked in electrolyte solution in two separate polypropylene (PP) cells, as depicted in Fig.2.1(a). The surface area of the Pt sheet was about 100 mm^2. They were employed as charge collectors. The liquid volume in each cell was 50 ml.

One cell was kept at room temperature by a cold water bath (21 ^oC), and the temperature of the other cell was raised by a Corning PC-220 Hot Plate, with a constant rate of 3 ^oC/min. The temperature was monitored continuously by type-K thermocouples. The liquid phase in the two cells was connected by a salt bridge, which was 5 mm in diameter and 30 mm long. The open-circuit voltage between the two charge collectors, V, was measured by a National Instrument SCB68 data acquisition (DAQ) system. Figure 2.2(a) shows a typical V-ΔT curve. The temperature sensitivity of V, dV/dT, is shown in Fig.2.3 as a function of the temperature difference, ΔT. When the high-temperature cell reached about 60 ^oC, the two charge collectors were connected through an external resistor, R_0 = 250 Ω. A typical discharge curve is shown in Fig.2.2(b).

Reference experiments were performed by using a similar experimental setup with the NC disks being removed; that is, only the Pt charge collectors were tested.

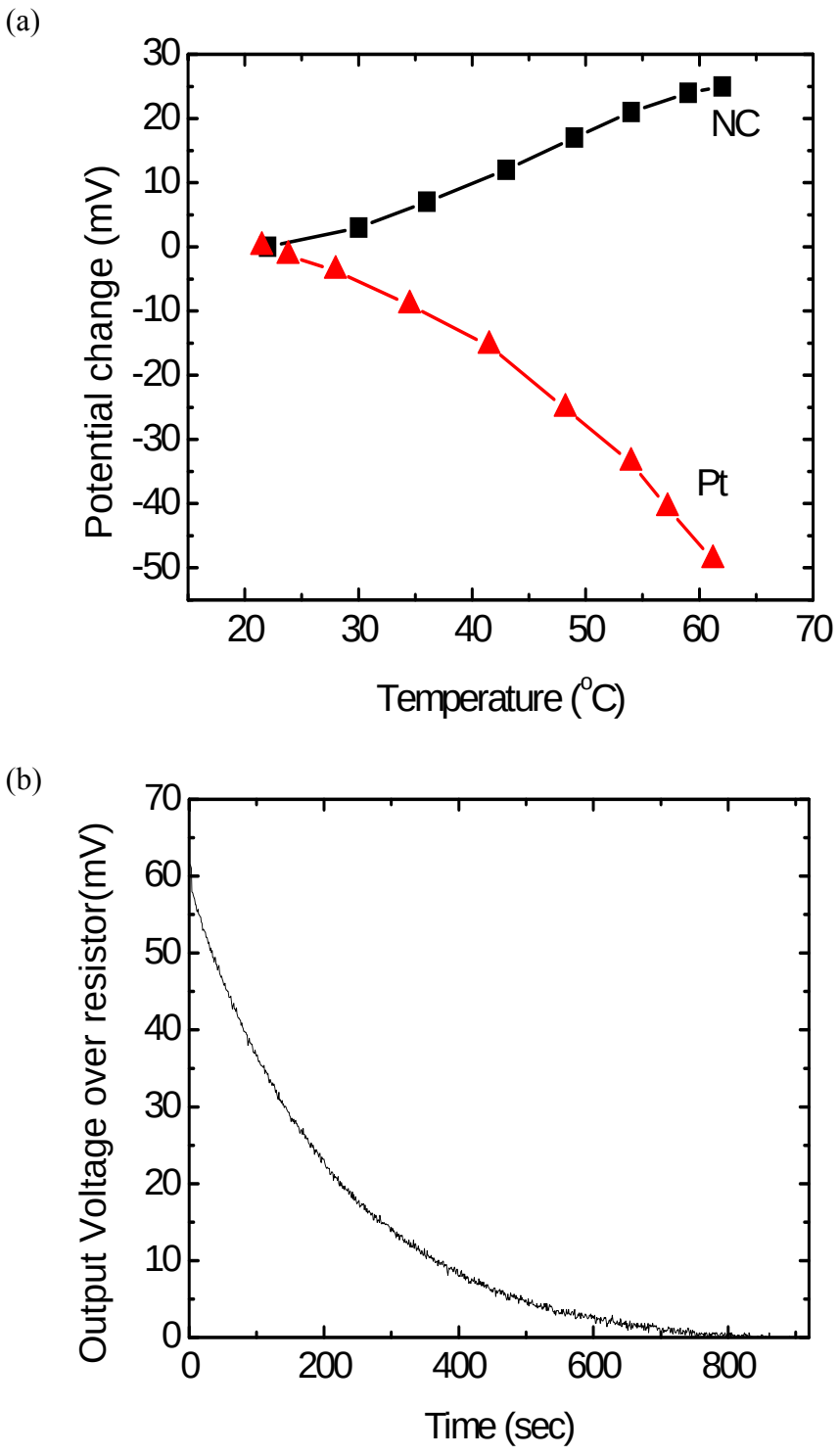

Fig.2.2. (a) Typical voltage-temperature curves of the nanoporous carbon(NC) and the charge collector(Pt), with the ion concentration being 1 M. (b) A typical discharge curve for the carbon based system, with $R_0 = 250\ \Omega$.

2.3.Results and Discussion

From the data of the NC based system in Fig.2.2 (a), it can be seen that as ΔT increases, the amplitude of the output voltage, $|V|$ rises monotonically. The value of $|V|$ reflects the electrode potential difference between the two electrodes, having contributions from both the NC disks and the Pt charge collectors. However, because the surface area of the Pt sheet is much smaller than that of the NC disk by a few orders of magnitude, its effective capacitance is negligible. As the Pt-liquid interface and the NC-liquid interface are in parallel, the output voltage should be governed by the NC phase. The magnitude of dV/dT of such as TCS is around 0.8 mV/^{o}C, much higher than the Seebeck coefficients of thermoelectric materials. When ΔT is only around 50 ^{o}C, the output voltage can be a few tens of mV.

During discharging, because the temperature does not vary, no thermal to electric energy conversion would happen. As the new equilibrium is reached, the output voltage vanishes as the electric energy is dissipated by R_0. The electric energy comes from the stored energy in the NC electrodes, harvested from LGH. The total energy can be calculated as $\int(V^2/R_0)dt$, with t denoting time. The graph in Fig.2.3(b) shows one example of energy harvesting from the cell with nonporous carbons immersed in 1M NaI water solution, the cell configuration of which is as depicted in the Fig.2.2(b). The testing data indicate that the energy density of the NC is more than 0.1 J/g, much higher than that of ordinary thermoelectric materials [54]. Clearly, LGH energy is harvested and stored as electricity.

Without the nanoporous phase, the reference system demonstrates quite regular characteristics. As ΔT increases, dV/dT is negative; that is, the electrode potential decreases, as it should, since at a higher temperature the solvated ions in the interface double layer are more mobile and the effective surface ion density becomes lower. When the two charge collectors are connected through the external resistor, the output voltage decreases instantaneously to zero and no output electric energy can be detected by using the current experimental setup, suggesting that due to the small surface area of the Pt sheet, the harvested and stored LGH energy is trivial.

As the ion concentration (C) increases, the dV/dT of the Pt sheet is reduced. At a large solid-liquid interface, anions are adsorbed on the electrode surface and forms the inner Helmholtz plane (IHP) [55]. The electrode potential can be described as [56]: $\phi = (\phi_M - \phi_{IHP})+(\phi_{IHP} - \phi_b)$, where ϕ_M, ϕ_{IHP}, and ϕ_b are the potentials of the electrode surface, the IHP, and the bulk liquid phase, respectively. The potential drops can be expressed in terms of integral capacities (K); thus, $\phi = Q_M/K_{M\rightarrow IHP}+Q_d/K_{IHP\rightarrow bulk}$, where the Q_M is the charge on the metal electrode, and the Q_d is the one in the diffuse layer. The overall interface capacitance is $C_i = dQ_M/d\phi$. Note that $Q_M = Q_{CA}+Q_d$, with Q_{CA} being the charge associated with the specifically adsorbed ions, and, consequently, $1 = dQ_{CA}/dQ_M+dQ_d/dQ_M$. Therefore, $1/C_i = 1/K_{M\rightarrow IHP} - (1/ K_{IHP\rightarrow bulk})(dQ_{CA}/dQ_M)$. Since the IHP structure may be simplified as a monolayer, Q_{CA} is linear to the adsorption coverage (θ) : $Q_{CA} = \alpha\cdot\theta$, with α being charge amount of anions on 100% coverage. Hence, $d\phi = dQ_M/K_{M\rightarrow IHP} - \alpha d\theta/K_{IHP\rightarrow bulk}$. The second term is only related with the adsorption. Therefore, the contribution of adsorption to $d\phi_{CA}= \alpha d\theta /K_{M\rightarrow IHP}$.

As a first-order approximation, the adsorption behaviors can be described by a Temkin isotherm [57]: $\theta = \ln\beta C/f = (k_B T/B)\ln[W \cdot C \cdot \exp(H_o/K_B T)]$, where k_B is Boltzmann constant, W is a parameter related to the molecular and ion distributions in the surface layer and in the bulk phase, B is a system constant related to the heat of adsorption, and H_o is the heat of adsorption. Thus, $d\theta/dT = k_B \ln(W \cdot C)/B + (dH_0/dT)/B$. Consequently,

$$\frac{d^2\phi_{CA}}{dC dT} = \frac{1}{K_{M\to IHP}} \frac{k_B \alpha}{BC} \tag{1}$$

Equation (1) explains why the slope of the plot of dV/dT *vs.* C is positive, since the parameters at the right-hand side (RHS) are positive except $K_{M\to IHP}$ and α ($K_{M\to IHP}$ is a capacitance by anion adsorption and α is the amount of negative charges, therefore they are negative). Because the dV/dT at every concentration is negative, the temperature sensitivity of V ($|dV/dT|$) would be reduced as the ion concentration (C) becomes higher, which fits with the data of the reference experiments in Fig.2.3.

It is remarkable that the above analysis based on the classic interface theory does not capture the behaviors of NC. First, as shown in Fig.2.2 (a), dV/dT is positive, suggesting that the electrode potential increases with temperature, which may be related to the confinement effect of nanopore walls. To derive Eq.(1), it is assumed that the bulk liquid phase can be taken as the reference state. In a nanopore, such an assumption may no longer be valid, as the volume fraction of the interior is comparable with that of the interface zone, especially in the smallest nanopores that are of the largest specific surface areas and dominate the system behaviors. That is, there are at least two

competing processes that affect V: the variation in the effective adsorption coverage (θ) and the net ion diffusion along the axial direction. As T increases, even if θ still decreases, as the effective potential at the interior of nanpores may vary faster, the overall electrode potential can indeed be reduced, resulting in the measured positive temperature sensitivity.

Second, as the ion concentration changes over a wide range from 0.1 M to 3.7 M, as indicated by Fig.2.3, there is not a clear pattern of the variation in $|dV/dT|$. When C = 0.1 M, the temperature sensitivity of the effective electrode potential is nearly 0.86 mV/^{o}C; when C = 1 M, $|dV/dT|$ decreases to less than 0.75 mV/^{o}C. While the trend looks similar with the prediction of the classic surface theory, when C further increases to 3.7 M, the temperature sensitivity rises back to 0.88 mV/^{o}C. The tolerance of the voltage measurement is quite small (< 0.5%), and the significant changes in $|dV/dT|$ cannot be attributed to data scatter. This unique phenomenon may also be associated with the lack of bulk phase in nanopores. According to Eq.(1), when C is relatively small, $|d^2V/dCdT|$ tends to be large. That is, as the ion concentration is low, the effect of the decrease in adsorption coverage is more pronounced, which may dominate the system behavior and leading to a negative correlation between $|dV/dT|$ and C. With a relatively high ion concentration, the surface layer effect is saturated and the ion diffusion along the axial direction becomes more important. If the thermal sensitivity of the effective axial diffusion rate increases sufficiently fast with the ion concentration, the temperature dependence of the potential at the interior would be reduced rapidly, so that the overall $|dV/dT|$ increases.

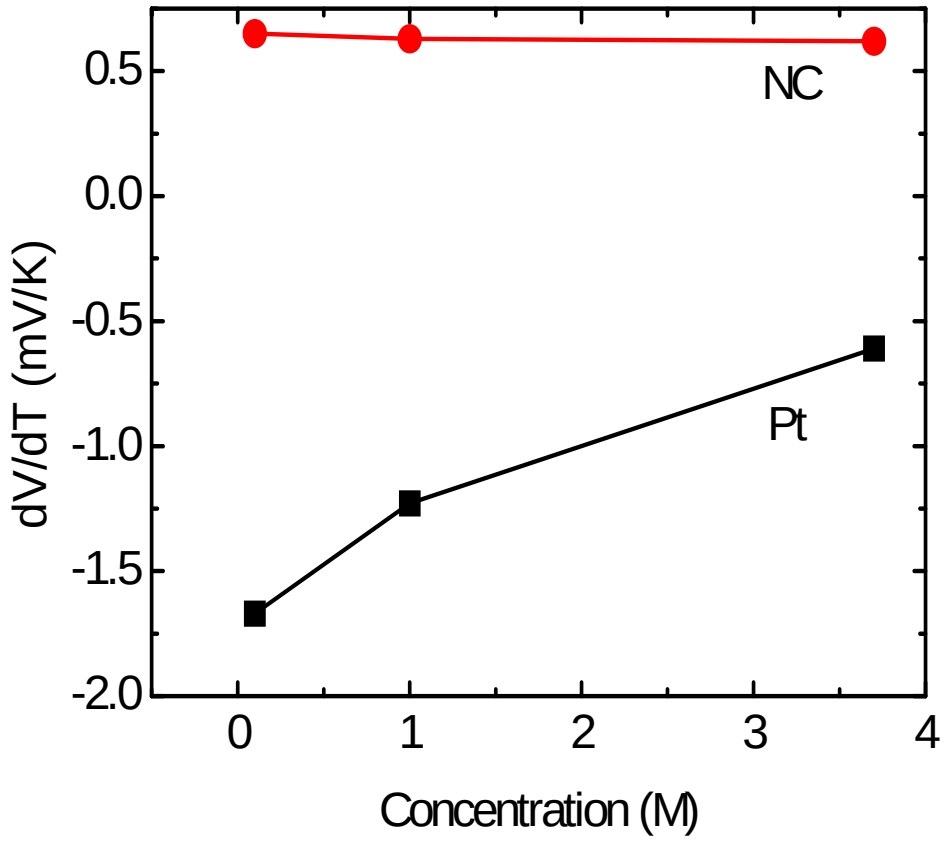

Fig.2.3. The temperature sensitivity of NC and Pt (d*V*/d*T*) as a function of the ion concentration.

2.4. Concluding Remarks

It is clear that the above analysis is merely a qualitative, zero-order analysis of the thermal dependence of confined ion behaviors. It does not facilitate a fully developed model. Nevertheless, the experimental data validate that the thermally induced capacitive effect can be employed for LGH harvesting and storage. The thermal sensitivity of electrode potential can be much larger than the Seebeck coefficients of thermoelectric materials. As this effect is amplified by the large specific surface area of nanoporous materials, the energy density of TCS can be quite high. As temperature rises, the electrode potential of the nanoporous carbon under investigation increases, and its thermal sensitivity ($|dV/dT|$) does not decrease monotonously, which are contradictory to the predictions of conventional surface theory. These unique phenomena may be related to the lack of bulk phase in the confining nanopore environment.

CHAPTER 3. Dependence on Cation Size of Thermally Induced Capacitive Effect of a Nanoporous Carbon

3.1. Introduction

Harvesting and storing low-grade heat (LGH) is of both significant scientific interest and important technological relevance. Usually, LGH refers to the thermal energy of relatively low temperature below 250 ^{o}C [58]. Every day, in the U.S. alone, many hundreds of Giga-Watt of power is being wasted as LGH in coal and nuclear power plants [59]. Other LGH sources include solar thermal energy, geo-thermal energy, ocean thermal energy, wasted heat in vehicles, and even body temperature of human beings. If LGH can be utilized with high energetic and economic efficiency, energy security can be much improved and energy-related emission can be greatly reduced.

Conventional thermal energy harvesting and storage techniques do not work well for LGH [e.g. 59, 60]. A major problem is the low energy density, making direct thermal energy storage methods, e.g. those based on phase transformations and/or chemical reactions [61], irrelevant. An intrinsic difficulty of converting LGH to electricity comes from the low temperature, which leads to the low Carnot cycle limit, ζ_c. Thus, the overall energy conversion efficiency $\zeta = \zeta_c \cdot \zeta_s$ tends to be poor, with ζ_s being the intrinsic system efficiency. For large-scale LGH sources, neither direct energy conversion, e.g. thermoeletrics, nor indirect energy conversion, e.g. Organic Rankin Cycle (ORC) machines and turbine engines, can work efficiently [62]. To overcome these hurdles, new mechanisms must be investigated.

Converting thermal energy to electric energy must be based on processes that are both thermally and electrically related. Such processes usually involve multiple phases/matters and take place at their interfaces. For a beneficial interface phenomenon, using nanostructured materials of ultrahigh specific surface areas ($A \sim 10^2$ to 10^3 m^2/g) can greatly amplify it. And, among all the interfaces, solid-liquid interfaces should be given a high priority as they are quite controllable. A nanostructured-materials-based device that uses solid-liquid interfaces to store electric energy is essentially a double-layer supercapacitor (DLS). For instance, when two identical nanoporous electrodes are soaked by an electrolyte solution and an external voltage is applied across them, the cathode would adsorb anions and the anode would adsorb cations. The stored charge can be assessed as $Q = Q_e \cdot A$, where Q_e is the effective surface ion density. Due to the large value of A, Q can be much higher than that of conventional capacitors [41].

Note that the ion adsorption of DLS is also thermally dependent. It is well known that a "poorly designed" DLS can lose up to 20% of its capacitance with a small temperature variation of 30-40 ^oC [63]. While this is usually regarded as a detrimental effect, recently we showed that its inverse process can be employed to harvest and store LGH as electric energy, leading to the development of the thermally-chargeable supercapacitor (TCS) technology [64]. The basic working mechanism of TCS is associated with the thermally induced variation of electrode potential. As depicted in Fig.3.1, a possible structure of TCS consists of two identical half-DLS. Each half-DLS is formed by immersing a nanoporous electrode in an electrolyte solution. As they are placed at different temperatures (T), there would be a potential difference (V) between them, because the effective surface ion density changes with T. Since the temperature

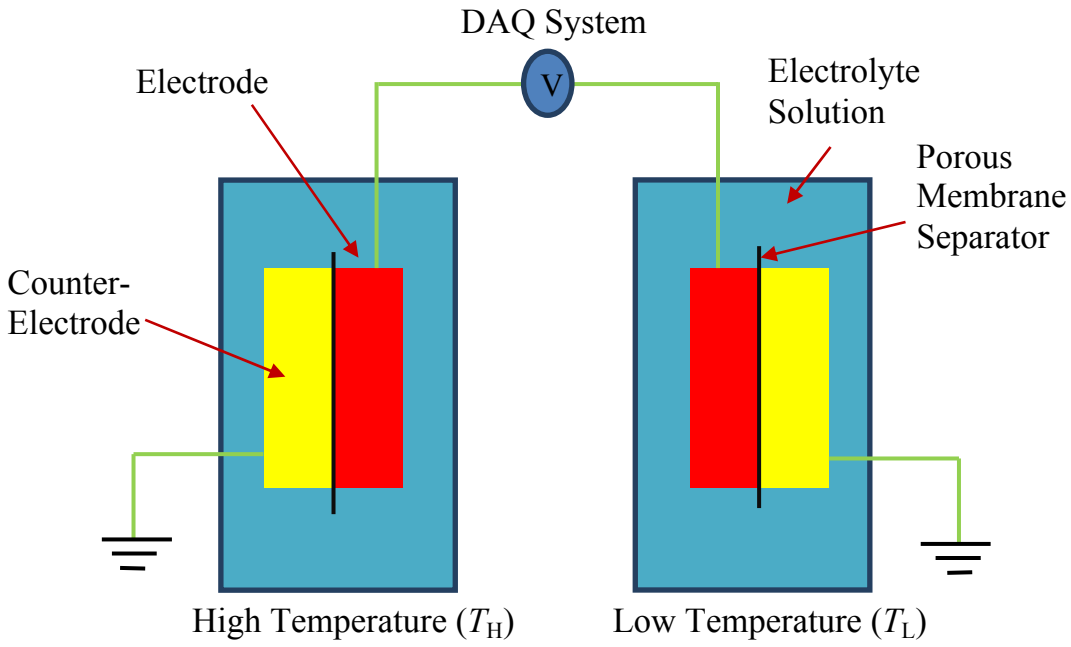

Fig.3.1. Schematic of a thermally-chargeable supercapacitor (TCS), consisting of two double-layer (DL) supercapacitor type cells. The counter-electrodes are separated from the electrodes by porous membrane separators, and are grounded either externally or internally. The output voltage (V) is measured by the data acquisition (DAQ) system.

sensitivity of electrode potential, $|dV/dT|$, is much higher than the Seebeck coefficients of thermoelectric materials, a TCS can have a high energy density. Moreover, as the two half-DLS are separated, the direct thermal conduction between them can be minimized, so that thermal shorting, the key factor that causes the low energetic efficiency associated with the Seebeck effect [65], is significantly reduced.

While the preliminary data have shown encouraging results, in order to optimize TCS a large number of technical and scientific questions must be answered. A critical one is: How to choose the electrolyte? Since compared with the anion effect, the cation effect, particular the influence of cation size, can be more important, it will be the focus of the current research.

3.2. Experimental

The electrode under investigation was formed by Cabot BP2000 nanoporous carbon (NC). The material was first refluxed in a vertical reactor in aceton for 4 h. The refluxing temperature was kept at 60^{o}C by a hot mantle. After vacuum drying at 80 ^{o}C for 8h, the treated NC powders were compressed into thin disks by a type-5580 Instron machine in a stainless steel mold. The mass of each disk was nearly 200 mg. The compression pressure was 400 MPa. By using a Micrometrics ASAP-2000 Analyzer, it was measured that the compressed carbon had a broad pore size (D) distribution from 1 nm to 100 nm, with the modal value at about 3 nm. The smallest nanopores with $D < 10$ nm contributed to more than 85% of the surface area.

The experimental setup was similar with Fig.3.1, except that the counter-electrode and the grounding connections were replaced by a salt bridge between the two

containers. The diameter of the salt bridge was 5 mm and the length was 30 mm. The two containers were made of polypropylene (PP). Each container contained 50 ml of aqueous solution of electrolyte, in which the treated NC disks were immersed. The electrolyte concentration was either 0.1 M or 3.7 M. The electrolyte was either lithium chloride (LiCl), sodium chloride (NaCl), potassium chloride (KCl), or cesium chloride (CsCl).

The two NC disks were connected to a National Instrument SCB68 data acquisition (DAQ) system by platinum (Pt) wires through two Pt charge collectors. One container was maintained at room temperature by a water bath. The other container was heated by a corning PC-220 Hot Plate, with the heating rate of 3 ^{o}C/min. The DAQ system continuously recorded the potential difference between the high-temperature and the room-temperature NC disks. Figure 3.2 shows the typical measurement results. The average dV/dT is shown in Fig.3.3 as a function of the cation size (d), with the ion concentration (C). According to the literature data [66], the cation sizes of Li^+, Na^+, K^+, and Cs^+ are 0.180 nm, 0.232 nm, 0.304 nm, and 0.362 nm, respectively.

3.3. Results and Discussion

Figure 3.2 indicates clearly that the effective electrode potential of the NC disk is highly sensitive to temperature, T, for all the tested chloride salts. Initially, when both containers are at room temperature, the potential difference is zero, as it should be, since the two NC disks are identical. When the temperature difference (ΔT) increases,

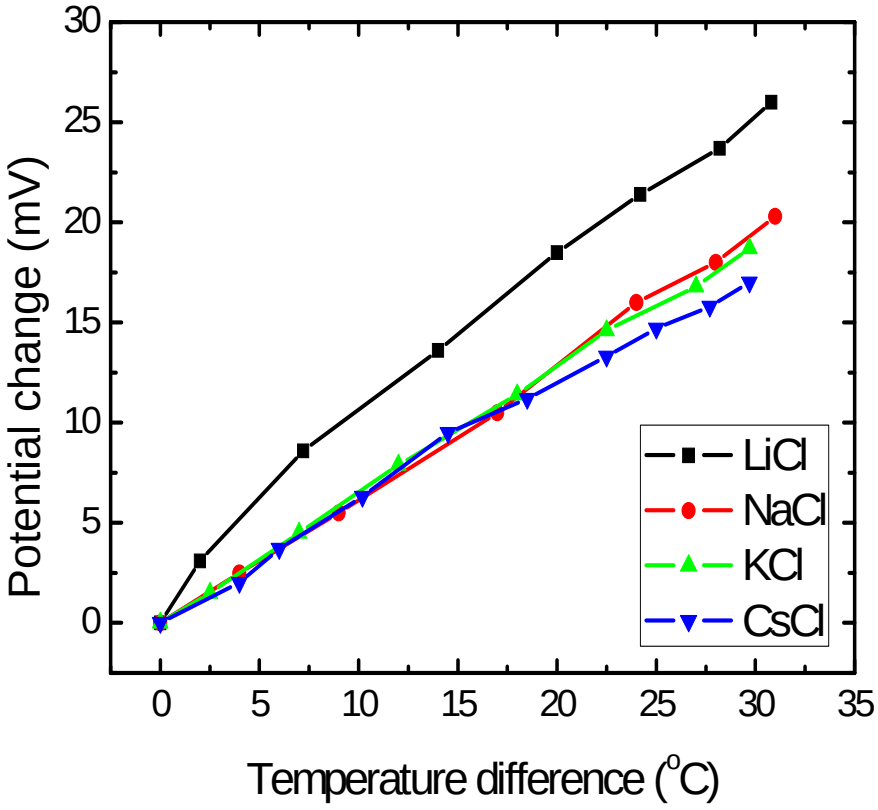

Fig.3.2. Typical results of the output voltage (V) as a function of the temperature difference (ΔT). The ion concentration is kept as 0.1M.

the electrode potential of the room-temperature NC disk remains constant, while that of the high-temperature NC disk rises, causing the measured output voltage (V).

The increase in V is a unique phenomenon somewhat contradictory to the prediction of conventional interface theory. At a large electrode surface, usually at a higher temperature the effective surface ion density is lower, as more ions can diffuse away from the inner Helmholtz plane (IHP) [67]. The opposite variation in electrode potential of the NC disk may be related to the confined ion structures in nanopore, where, when temperature rises, not only the adsorption coverage of IHP changes, but also the overall ion distribution in the interior would vary. The former is well captured by classic interface models [e.g. 68], while the latter is often assumed constant. For the NC disks, the net output voltage is determined by the two competing factors. If the latter dominates, dV/dT tends to be positive; and vice versa.

First of all, we noted that the sign of the dV/dT is positive. This means that the moving ion specie associated with the output voltage change is primarily a cation not an anion. Because the activated carbon usually has acidic functional groups such as hydroxyl or carboxylic ones on its surface, they can keep the anion from entering its pores. [69]

Recently, we made a report about the temperature dependence of electrode potential when specific adsorption of ions exists. In the report we derived one equation about dV/dT based on Temkin's isotherm.[70] $\frac{\mathrm{d}\phi}{\mathrm{dT}} = \frac{1}{K_{\mathrm{M}\to\mathrm{IHP}}}\left\{\frac{\alpha k_{\mathrm{B}}}{B}\ln(W \cdot C) + \frac{1}{B}\frac{dQ_0}{dT}\right\}$,where $K_{\mathrm{M}\to\mathrm{IHP}}$ is the integral capacity from metal to Inner Helmholtz Plane, k_{B} is the Boltzmann constant, B is a system

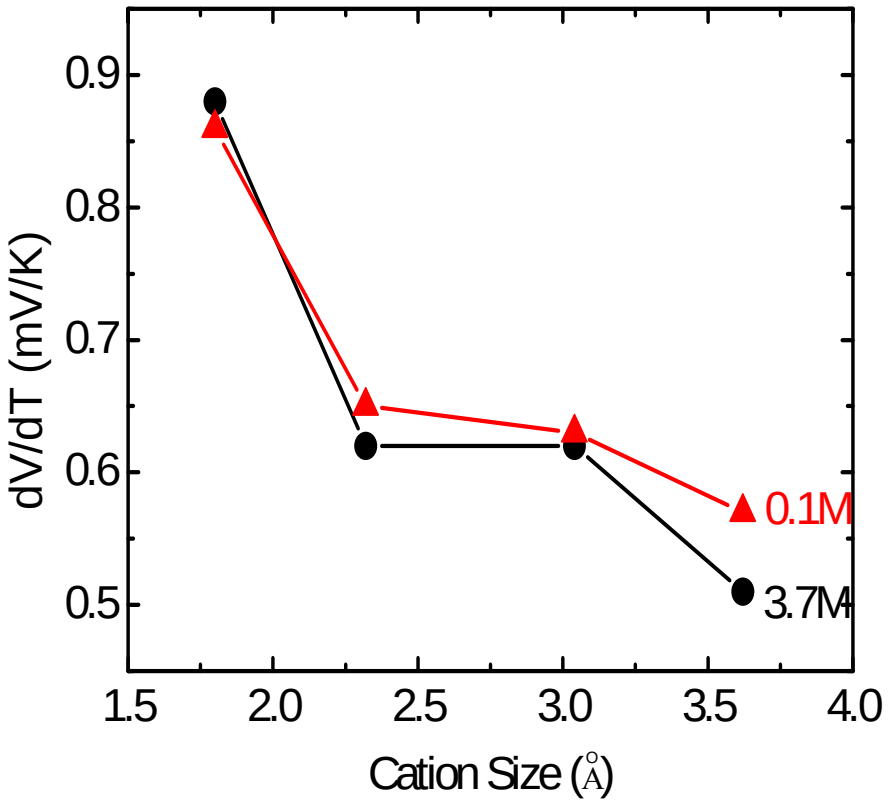

Fig.3.3. The average values of |d*V*/d*T*| as a function of the cation size, *d*.

parameter, W is dependent on the distribution of ions, and Q_o is the heat of adsorption. [71]. According to this relation, the dV/dT should increase with ion size. [72] However, as in Fig.3.3, the dV/dT decreased with increasing ion size. This result says that the tested cations were not specifically adsorbed on the electrode surface. It is well know that alkali metal ions cannot be specifically adsorbed, because the process is thermodynamically unfavorable. [73]

The temperature sensitivity of electrode potential is dominated by the surface ion behaviors, strongly affected by the ion properties. The factor of cation size can come in through a few effects. First, the solvated structure is a function of the cation size. For a smaller cation, with the same ion charge, the coordination number of the hydration shell is smaller, which affects the effectiveness of inducing counter charges in the electrode surface (Q_M). On the one hand, as the increase in Q_M raises the electrode potential, the absolute value of dV/dT would be larger even when the portion of varied surface charges is the same. On the other hand, a higher electrode potential causes a higher energy barrier for the surface ions to diffuse away from OHP, which may reduce the effects of temperature increase. Second, usually the cation mass (m) and the cation size (d) are correlated; a smaller cation tends to be more lightweight. With a larger m, a cation is less mobile while its ability to overcome energy well is lower. Other important issues include the interaction among solvated cations, anions, and water molecules, the distribution of cations along the radius and the axial directions in nanopores, the distortion of hydration shells, etc.

These factors affect the system performance simultaneously, competing against each other. As some of them tend to lower the temperature sensitivity of electrode potential and the others tend to increase it, there may exist a critical cation size at which $|dV/dT|$ is maximized. When the cation size is relatively small, the influences of cation mass are pronounced, and $|dV/dT|$ may increase with d. If the cation size is relatively large, the influence of solvated structure may be important, and $|dV/dT|$ tends to decrease as d further increases.

However, the experimental data in Fig.3.3 suggest that for the nanoporous carbon and the chloride salts under investigation, the temperature sensitivity of electrode potential decreases monotonically as the cation size increases, even for the smallest lithium and sodium ions. In the tested samples, the NC disks are identical and the solvent, the cation charge, the anion specie (Cl^-), the ion concentration are all the same. The only major difference is the cation size. For both dilute (0.1 M) and high-concentration (3.7 M) solutions, $|dV/dT|$ is nearly 0.85 mV/^{o}C for lithium salt, and decreases to about 0.52 mV/^{o}C for the largest cesium salt, by almost 40%. The relationship between $|dV/dT|$ and d is quite nonlinear. When the cation changes from lithium to sodium and from potassium to cesium, the decrease in $|dV/dT|$ is quite evident. The difference between sodium and potassium cations is within the tolerance of the measurement.

This phenomenon should be associated with the influence of nanopore walls. In a nanopore, particularly in the smallest micropores ($D < 2$ nm) that contribute most to the specific surface area and dominate the system performance, the space is insufficient

for fully developed hydration shell clusters. Not only the distribution of solvated ions would change, but also the molecular configuration of each shell is different [74,75]. Thus, the above analysis for large surfaces breaks down. Moreover, in such a small nanopore, there is no bulk phase and the entire confined liquid phase is exposed to the solid atoms. The equilibrium between the OHP and the interior may not be reached, as the ion diffusion along the axial direction has different characteristic time scales [76]. As the cation size increases, the hydration shell tends to swell and the confinement effect of nanopore walls is more pronounced, and the "shear" force that the hydration shell must overcome to slide against the nanopore surface is larger [77]. As the excess ions are effectively less mobile, the confined ion structure is less sensitive to the temperature change, so that $|\mathrm{d}V/\mathrm{d}T|$ is lowered. When the cation size is relatively small, the interaction among adjacent hydration shells is anisotropic. In the intermediate range of cation size, such an effect is somewhat reduced; thus, the electrode potentials of sodium and the potassium ions tend to have similar thermal sensitivity. For larger cations, the distortion of the hydrations hells is significant and $|\mathrm{d}V/\mathrm{d}T|$ continues to decrease.

3.4. Concluding Remarks

Clearly, detailed analysis on thermally induced ion transport in nanopores must be carried out to fully understand the TCS performance. The current experimental research merely raises the question, instead of answering it, that the confinement effects of nanopore walls may be critical to the thermal sensitivity of electrode potential.

Nevertheless, the testing data have showed that using different cations can significantly affect the TCS properties. When the cation size increases, with everything else being the same, $|dV/dT|$ decreases. The decrease in $|dV/dT|$ is more pronounced when the cation size is relatively small or large, compared with the intermediate range of d. This finding may open a new area of study for the eventual system optimization.

CHAPTER 4. Anion Size Effect on Electrode Potential in a Nanoporous Carbon

4.1. Introduction

While it has been well known that low-grade heat (LGH) is ample, currently there is still no satisfactory technique that can efficiently harvest and store it [e.g. 48]. By definition, the temperature of LGH is usually lower than 250 ^{o}C. Important LGH sources include the coolants in coal and nuclear power plants, solar thermal energy, geothermal energy, ocean thermal energy, wasted heat in vehicle engines, among others. Due to the low energy density, ordinary thermally triggered phase transformations and chemical reactions are inefficient for LGH storage [78]. Moreover, directly storing thermal energy imposes tough challenges to thermal insulation and energy transportation, and is inconvenient to utilize the energy in other forms.

The major technical difficulties associated with converting LGH to electricity are caused by the relatively low temperature, T. The Carnot cycle efficient is $\zeta_c = \Delta T/T$, with $\Delta T = T - T_r$ and T_r being the reference temperature. For LGH with T in the range of 80 ^{o}C to 200 ^{o}C, ζ_c is only ~20% to ~ 40%. Thus, the system efficiency, ζ_c must be very high so that the overall energetic efficiency $\zeta = \zeta_c \cdot \zeta_s$ can be sufficient. However, both direct energy conversion of thermoelectric materials and indirect energy conversion of Organic Rankin Cycle (ORC) engines do not work for LGH as efficiently as for higher temperatures [79], leading to high power costs around a few to tens of dollars per Watt [80]. The indirect energy conversion methods also demand sophisticated supporting

components such as pumps, heat exchangers, etc. that have a large number of moving parts, further much increasing the installation, maintenance, and operational costs [81].

Recently, in an experimental study on nanoporous materials [64], we demonstrated that, except for the classic Seebeck effect, other thermally and electrically related processes can be employed for direct energy conversion, e.g. the thermally affected capacitive effect that will be investigated in the current research.

As an electrode is in contact with an electrolyte solution, its surface would be spontaneously electrified as a certain amount of ions are adsorbed [82]. The surface ion layer is formed by the anisotropic force fields from the solid phase and from the liquid phase, characterized by the adsorption coverage (θ). Since the inner Helmholtz plane (IHP) can often be regarded as a monolayer of solvated ions, the induced surface charge is linear to the adsorption coverage: $Q_e = \alpha \cdot \theta$, where α is a coefficient dependent on the ion and electrode properties. The double-layer structure of surface charges leads to an electrode potential (ϕ) normal to the solid-liquid interface. When temperature rises, due to the variation in ion mobility, the adsorption coverage becomes different, and the surface charge and the electrode potential would also change. As the electric field varies, a certain amount of electric energy is effectively stored in the system, which is converted from the consumed thermal energy. When this capacitive effect is greatly amplified by the large surface area of a nanoporous electrode, the energy density can be very high. Such a system, in essence, becomes a thermally chargeable supercapacitor (TCS), which works in the temperature range of LGH (the working temperature is limited by the boiling point of the electrolyte solution).

The TCS performance is dependent on a large number of system parameters, such as the surface area and properties of electrode materials, the grounding structure, the working temperature range, as well as the liquid phase. Previously, we investigated the influences of the ion concentration [71] and the cations [83]. In this paper, we will analyze the anion effects.

4.2. Experimental procedure

The experimental setup is depicted in Fig.4.1. In two polypropylene (PP) containers, two identical electrodes were immersed separately. The electrodes were made of Cabot BP2000 nanoporous carbon (NC) powders. The NC sample was first refluxed with aceton in a vertical apparatus consisted of a round-bottom flask and an Allihn condenser. The temperature was maintained at 80 ^{o}C by a thermal mantle for 4 h, followed by drying in a VWR 1410 vacuum oven at 80 ^{o}C for 12 h. Then, about 200 mg of NC powders were compressed in a stainless steel mold by a type 5580 Instron machine at 400 MPa for 5 min, forming an electrode disk. By using a Micrometritics TriStar-3000 Gas Absorption Analyzer, a Brunauer-Emmett-Teller (BET) analysis was performed and the specific surface area was measured as 1810 m^2/g. The nanopore size had a relatively broad distribution from the lower end of the mesoporous range (2 nm) to the lower end of the macroporous range (~100 nm), with the modal value at about 3 nm. Each electrode contained a NC disk and a platinum (Pt) foil charge collector that were firmly compressed together. The surface area of each Pt foil was $1cm^2$. The electrodes were soaked in an electrolyte solution. The potential difference between the

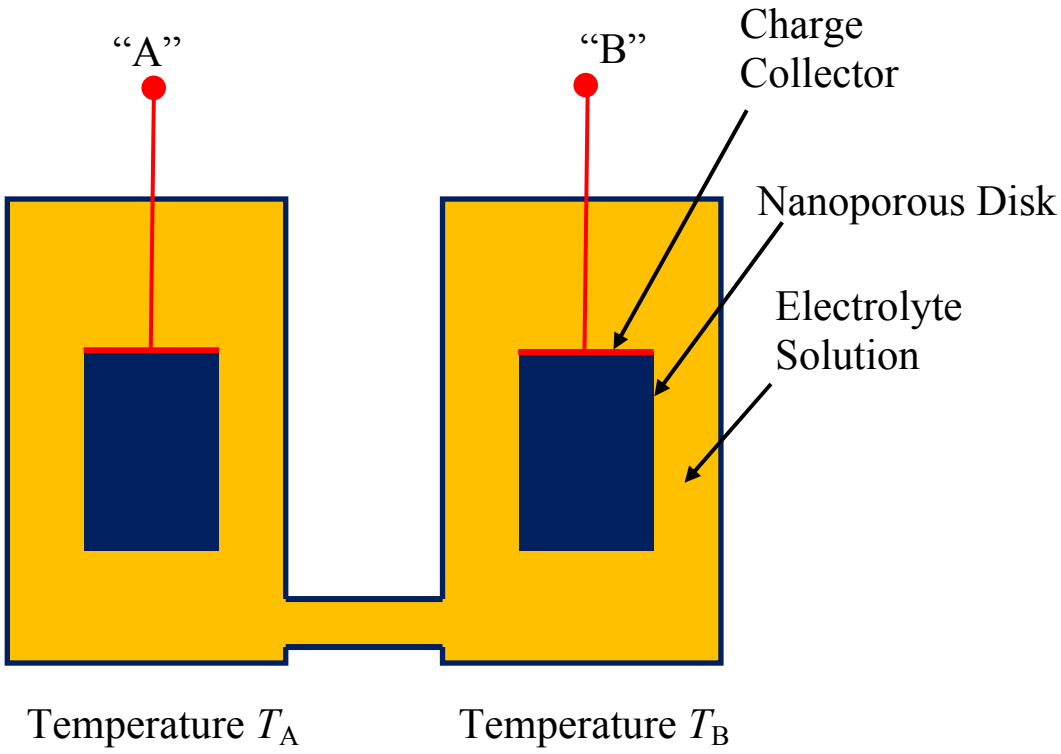

Fig.4.1. Schematic of a TCS, formed by two half-DLS at different temperatures.

two electrodes (V) were measured between "A" and "B" by a National Instrument SCB-68 Data Acquisition (DAQ) system. The components were connected by Pt wires. The circuit was completed by a salt bridge between the two containers. The diameter and the length of the salt bridge were 5 mm and 30 mm, respectively. By using a corning PC-220 hot plate, the liquid phase in one of the containers was heated slowly, with a constant heating rate of 3 ^{o}C/min. The other container was kept at 21 ^{o}C by using a cold water bath. The liquid phase was a 1 M aqueous solution of sodium salt. The solute was either sodium fluoride (NaF), sodium chloride (NaCl), sodium bromide (NaBr) or sodium iodide (NaI). Figure 4.2 shows the typical output voltage, through which the average temperature sensitivity of output voltage (dV/dT) can be calculated, as shown in Fig.4.3.

Reference experiments were carried out on the charge collectors. The setup was similar with the NC system, except that the two NC disks were removed. The testing results of V and dV/dT are also shown in Figs.4.2 and 4.3.

4.3. Results and discussion

All the tested samples are of the same electrode materials, solution (water), ion concentration (1 M), cation (Na^{+}), and anion charge. The only difference among them is the anion specie, particular the anion size (D). According to literature data, the anion sizes for F^{-}, Cl^{-}, Br^{-}, and I^{-} are 0.238 nm, 0.334 nm, 0.364 nm, and 0.412 nm, respectively. In the reference system, the electrode is the metallic foil. Initially, when the temperatures of both containers are the same, the output voltage is zero, since both

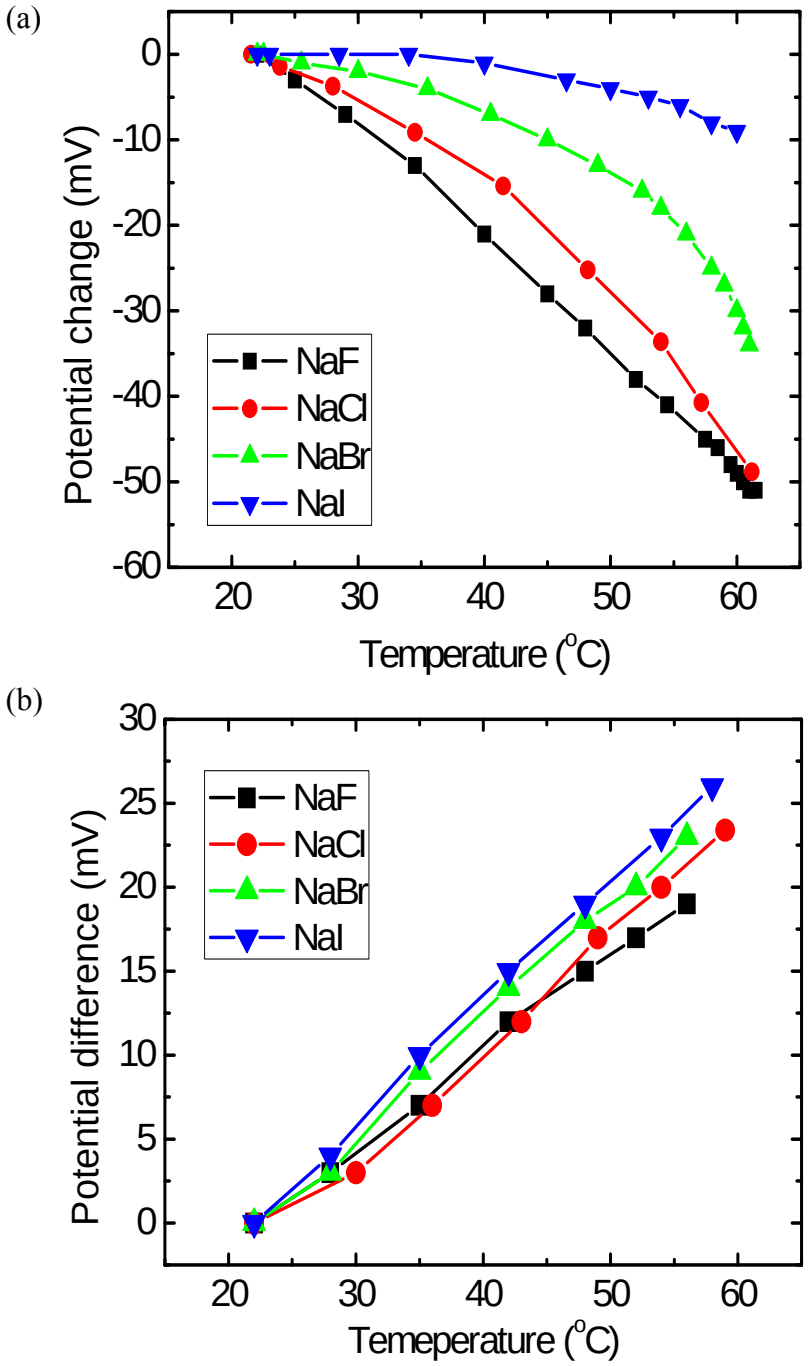

Fig.4.2. Typical results of the output voltage (V): (a) The reference system; and (b) The nanoporous carbon system. The ion concentration is 1 M.

sides have the same electrode potential. As the temperature of one container (T) increases, the electrode potential became more negative, which means the density of anion near the interface is decreasing, that is, the anions are desorbing from the electrode surface. According to the classic Temkin isotherm [70], $\theta = (k_BT/B)\ln[W{\cdot}C{\cdot}\exp(Q_o/k_BT)]$, where k_B is Boltzmann constant, W and B are system parameters related to the molecular and ion distribution and a system constant (B>0), respectively and Q_o is the heat of adsorption. The electrode potential can be derived as [83]: $\phi = (1/K_{M\rightarrow IHP}+1/K_{IHP\rightarrow bulk})\beta\theta$, where $K_{M\rightarrow IHP}$ and $K_{IHP\rightarrow bulk}$ are the integral capacitances of from electrode to IHP and from IHP to bulk solution, respectively; β is charge amount when the surface is fully covered dependent on the interaction among solid atoms, solvent molecules, and solvated ions. Since the reference temperature (T_r) is constant, $dV/dT = d\phi/dT$. Thus,

$$\frac{dV}{dT} = \frac{1}{K_{M\rightarrow IHP}} \cdot \left\{\frac{k}{B}\ln(W \cdot c) + \frac{1}{B}\frac{dQ_0}{dT}\right\} \qquad \text{Eq (1)}$$

,with c being the ion concentration. In our test with planar Pt electrode, the temperature sensitivity was increased with smaller anion. This phenomenon states that the adsorption behavior of the smaller anion is more sensitive to temperature change. As shown in the eq. (1), the temperature dependence of the heat of adsorption (dQ_0/dT) affects the temperature sensitivity of the electrode potential. It was reported that molecular shape and size has an effect on the dQ_0/dT. [84] Likewise, we speculate that the anion size also affect the second term in the eq. (1). The dQ_0/dT is, in

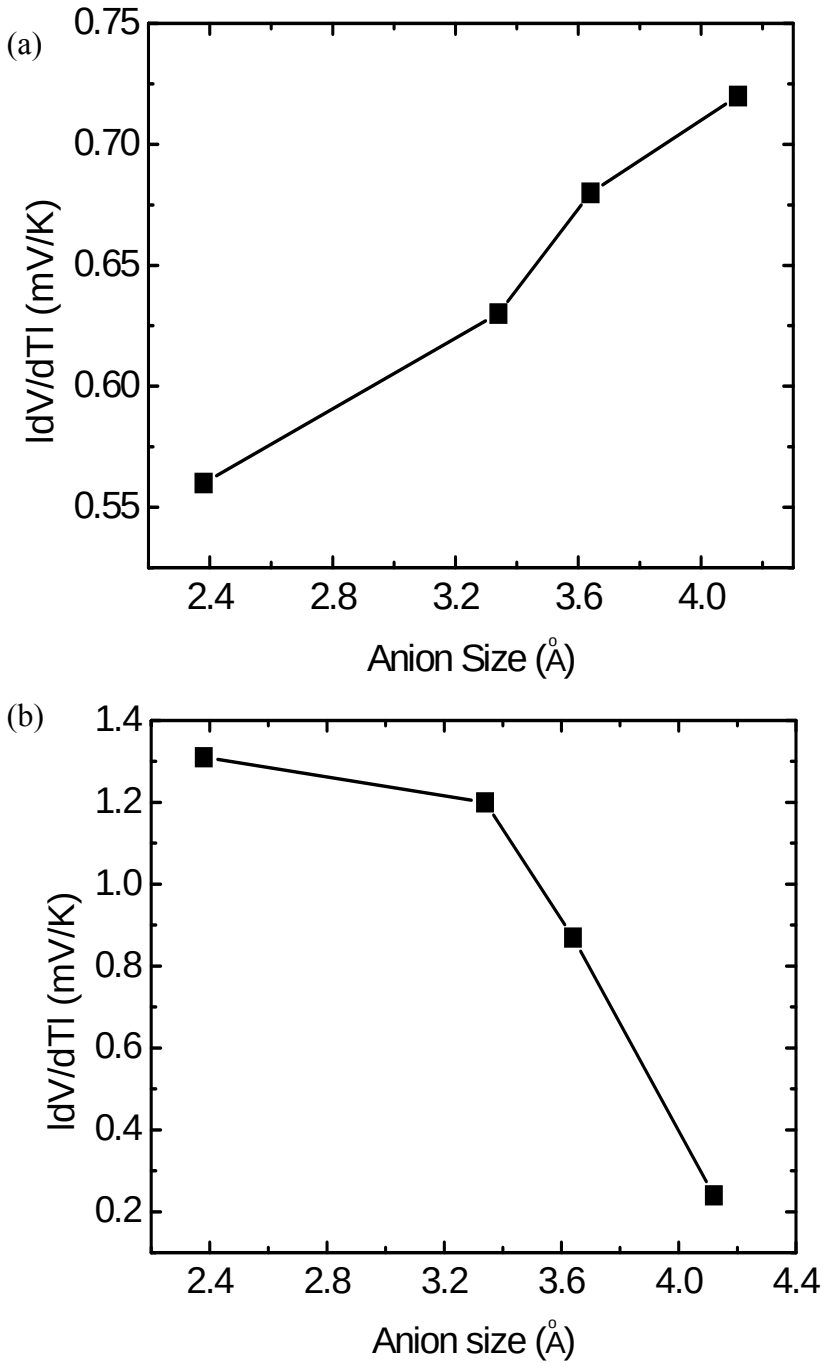

Fig.4.3. The temperature sensitivity of electrode potential ($|dV/dT|$) as a function of the anion size, d: (a) The nanoporous carbon system; and (b) The reference system.

thermodynamic sense, defined as a change in heat capacity (ΔC) before and after the adsorption. [69] Before the adsorption, the anion is solvated with several water molecules. When it's adsorbed on the surface, it loses some part of hydration shell. This makes the difference in the C. Because smaller anion has higher hydration number and the change in hydration number should be more than that in larger anion case. [85] As a result, the dQ_0/dT of smaller anion should be higher than that of bigger anion, and the dV/dT should so. This reasoning is compatible with the test result with Pt foil electrode in Fig.4.3(b).

As NC disks are added in the system, due to their large capacitance associated with the ultrahigh surface area (10^6 times larger than the surface area of the Pt foil), they would dominate the measured output voltage (V), as the contribution from the charge collectors is trivial. It can be seen that, dV/dT is positive; that is, the effective electrode potential increases with temperature, which is contradictory to the prediction of the classic theory discussed above. This unique phenomenon may be related to the lack of bulk liquid phase in nanopores; i.e. the interior cannot be regarded as a reference state. Usually, activated carbon has acidic functional groups such as hydroxyl or carboxylic surface group on its surface. Such negatively charged functional groups hinder anion's entrance into the nanopore. [86] The primary change in ion density with increasing temperature is in that of cations, hence, the dV/dT has the positive sign. The desorbed cations must diffuse along the axial direction of nanopores to reach the ion reservoir outside the pore, which has different characteristic time scales from the electrode potential change. As temperature increases, both the adsorption coverage and

the diffusion characteristics would vary. If the latter changes faster than the former, even when the effective θ decreases, the overall electrode potential may still increase.

Another interesting phenomenon is, when the anion size increases, the electrode potential becomes more thermally sensitive, and dV/dT increases. For the smallest anion of F^-, dV/dT is around 0.53 mV/^{o}C; as the anion size becomes larger (Cl^-), dV/dT increases to nearly 0.63 mV/^{o}C; when the anions are the even larger Br^- and the largest I^-, dV/dT are ~0.67 mV/^{o}C and ~0.72 mV/^{o}C, respectively. The dV/dT-D relationship is somewhat linear. From the testing data shown in Fig.4.3(a), there is no clear evidence showing that whether the anion size effect is more pronounced when D is relatively small or large. This result cannot be explained by the classic theory that the system free energy associated with ion adsorption is smaller for larger anions [86,87] – As the IHP of larger anions tends to be more stable, its thermal sensitivity should be lower.

Even with the hindrance of the negative charges in the entrance of the nanopore, the anion seems to enter the pore and make the difference by its size effect. In a nanopore, due to the confinement effect, anions's specific adsorption can be enhanced, causing a "squeezing" effect [88]. The combined influences from both the cations and the anions may lead to the opposite trend in dV/dT change. Particularly, as the solvated structures of larger anions are less stable, stronger bonds may be formed with the solvated cations and/or water molecules. Such a larger-scale structure can be more sensitive to the temperature change, so that the variations in the adsorption coverage and the electrode potential are promoted. Another possible mechanism, similar with the above discussion on the ϕ-T relationship, is related to the confined ion diffusion in

nanopores. As the hydration shells of larger anions are relatively unstable, their thermally driven diffusion can be easier than that of smaller ones. Thus, the confined structures of smaller anions are farther away from the equilibrium, resulting in the reduced thermal sensitivity of effective electrode potential.

4.4. Concluding remarks

To summarize, through an experimental study on a nanoporous carbon based TCS, it is found that anion size has significant effects on the thermal sensitivity of electrode potential. Contradictory to the prediction of classic theories, the electrode potential increases with temperature, which may be attributed to the lack of bulk phase in nanopores. Moreover, $|\mathrm{d}V/\mathrm{d}T|$ increases with the anion size; that is, with everything else being the same, increasing anion size has a beneficial effect for enhancing the TCS performance. Qualitative discussions are given for these unique phenomena. The detailed mechanisms and processes are still under investigation.

CHAPTER 5. Thermal Sensitivity of electrode Potentials of A Few Metallic Materials

5.1. Introduction

To enhance energy security and to reduce energy-related emissions, it is critical to better utilize the energy that is currently being wasted and/or even regarded harmful. One of the important energy sources is low-grade heat (LGH), thermal energy with the temperature (T) lower than 200 ^{o}C to 300 ^{o}C [58], such as the wasted heat in coal and nuclear power plants, distributed solar thermal energy, geo/ocean-thermal energy, wasted heat in vehicle engines, etc. If LGH can be harvested, stored, and used with high energetic and economic efficiency, from coal power plants alone, many Giga-Watt of additional power can be generated in the U.S. [59]. For another example, today's best solar panels can convert only ~16% of solar energy to electricity [89]; the rest of energy is eventually dissipated as LGH. If the wasted LGH can be harvested with an efficiency of 5-8% (the Carnot cycle limit for solar panels is around 10%), the overall efficiency can be largely increased by nearly 50%.

However, the low temperature associated with LGH demands a very high system efficiency, which cannot be achieved by conventional thermal-to-electric energy conversion (TEEC) technologies, including the direct TEEC techniques based on the Seebeck effect and the indirect TEEC techniques such as Organic Rankin Cycle (ORC) machines and turbine engines [62]. The major issue of the indirect methods is the high cost, typically more than a few dollars per Watt [50], due to the low energy conversion efficiency and the high installation, maintenance, and operational costs associated with

the expensive supporting components and moving parts, such as pumps, heat exchangers, etc. The main technical difficulty of thermoelectric materials is thermal shorting; i.e. as electrons move from the high-temperature end to the low-temperature end and electric energy is generated, thermal conduction also occurs spontaneously [65]. Moreover, the energy density of thermoelectric materials is usually quite low [49].

Searching novel TEEC techniques that can work better for LGH has been an active area of study for the past decade [90]. A TEEC process must be based on one or multiple physical and/or chemical phenomena that are both thermally and electrically sensitive. Recently, in a preliminary research on thermally induced capacitive effect [91], we developed the technology of thermally-chargeable supercapacitors (TCS). In a TCS, two half-supercapacitors are placed at different temperatures, as depicted in Fig.5.1. Each half-supercapacitor consists of an electrode immersed in an electrolyte solution. At the solid-liquid interface, the solvated ions are subjected to anisotropic force fields and form a double layer, inducing counter charges in the electrode phase [67]. Thus, a certain amount of electric energy is stored as the surface charges. A potential difference is generated between the electrode and the liquid phase, which is often referred to as electrode potential. As temperature varies, accompanied by the change in effective surface ion density, the electrode potential would become different. Consequently, when the two electrodes in a TCS are connected, a net output voltage can be measured. If the electrode is a nanoporous material of an ultrahigh surface area (10^2-10^3 m^2/g), the capacitance of such a device can be quite high [19], leading to a high energy density. The TCS works in the LGH temperature range, below 100 ^oC if the

liquid phase is aqueous. Due to the high mobility of the surface ions, even with a small temperature difference of only a few tens of ^{o}C, the output voltage can be on the scale of 10^2 mV [19], higher than that of thermoelectric materials by more than an order of magnitude.

With a constant internal impedance, the harvested and stored electric energy by a TCS is proportional to V^2, where V is the net output voltage. It is clear that, in order to maximize the harvested LGH energy, the thermal sensitivity of electrode potential, dV/dT, must be as high as possible. This will be the focus of the current study.

5.2. Experimental

The experimental setup is shown in Fig.5.1. Two identical electrodes were immersed in a formamide (FA) solution of lithium chloride (LiCl). The ion concentration was 21%. The electrodes were foils of platinum (Pt), nickel (Ni), copper (Cu), or indium (In). The rational of choosing these materials will be discussed in the next section. The electrodes were placed in two 50 ml containers, separately. The containers were connected by a salt bridge, with the diameter of 5 mm and the length of 30 mm. By using a cold water bath, one of the containers was kept at room temperature (T_r). The other container was heated by a Corning PC220 heat plate, with a constant heating rate of 3 ^{o}C/min. The temperatures of the two electrodes were monitored by type-K thermocouples, with a National Instrument HH-20A Reader.

As the temperature difference between the two electrodes (ΔT) increased, a significant output voltage (V) was measured between the two electrodes by a National Instrument SCB68 data acquisition (DAQ) system. Figure 5.2 shows the typical V-ΔT

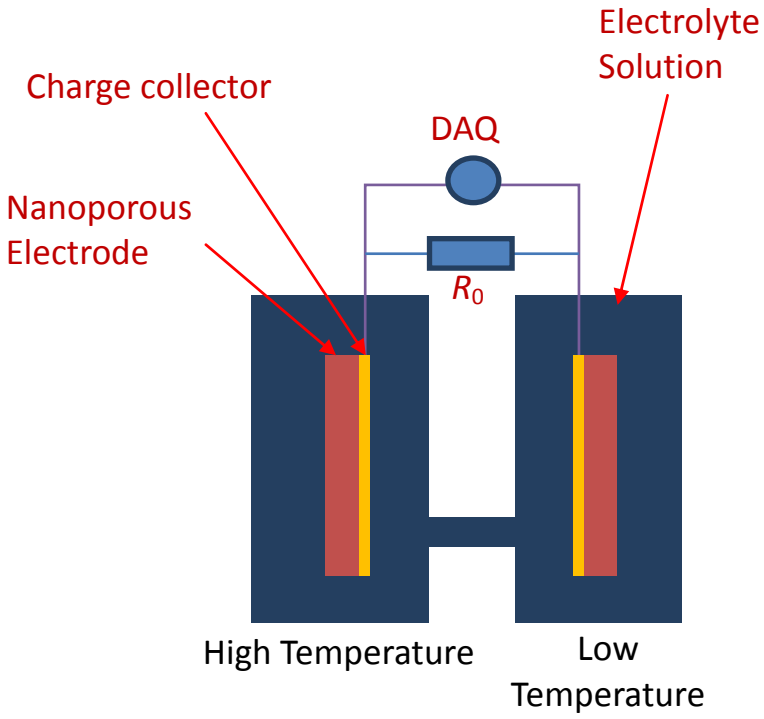

Fig.5.1. Schematic of a TCS, formed by two identical electrodes separately immersed in an electrolyte solution.

curves for the four materials under investigation, based on which the average thermal sensitivity of electrode potential (dV/dT) was calculated, as shown in Fig.5.3. For self-comparison purpose and for the sake of simplicity, the average dV/dT was taken as $V_{max}/\Delta T_{max}$, where V_{max} and ΔT_{max} are the maximum potential difference and the maximum temperature difference reached in the experiments, respectively. It qualitatively describes how rapidly the output voltage increases with temperature.

5.3. Results and Discussion

The experiment is so-designed because we speculate that the thermal sensitivity of electrode potential is related to the work function (WF) of the electrode material. Work funcition is a concept in Solid State Physics, defined as the minmum energy that is required to remove an electron from the Fermi level to vacuum [92]. For the metallic materials investigated in this study, the conduction band is partly filled and the Fermi level is inside the band [93]. The value of WF is typically a few eV, depending on a number of factors, such as the packing mode of atoms, the crystallographic orientation, etc. It is closely correlated to trhe ionization energy and insensitive to the surface charges. It can be calculated as WF = $W_d - E_F$, where W_d is the potential difference caused by surface dipole, and E_F is the Fermi energy. According to literature data [93], the values of WF of In, Cu, Ni, and Pt are 4.1 eV, 4.8eV, 5.2eV, and 5.5eV, respectively.

In the classic Gouy-Chapman model [94], the adsorbed ion structure at a solid-liquid interface is simplied as an electric double layer, consisting two capacitive

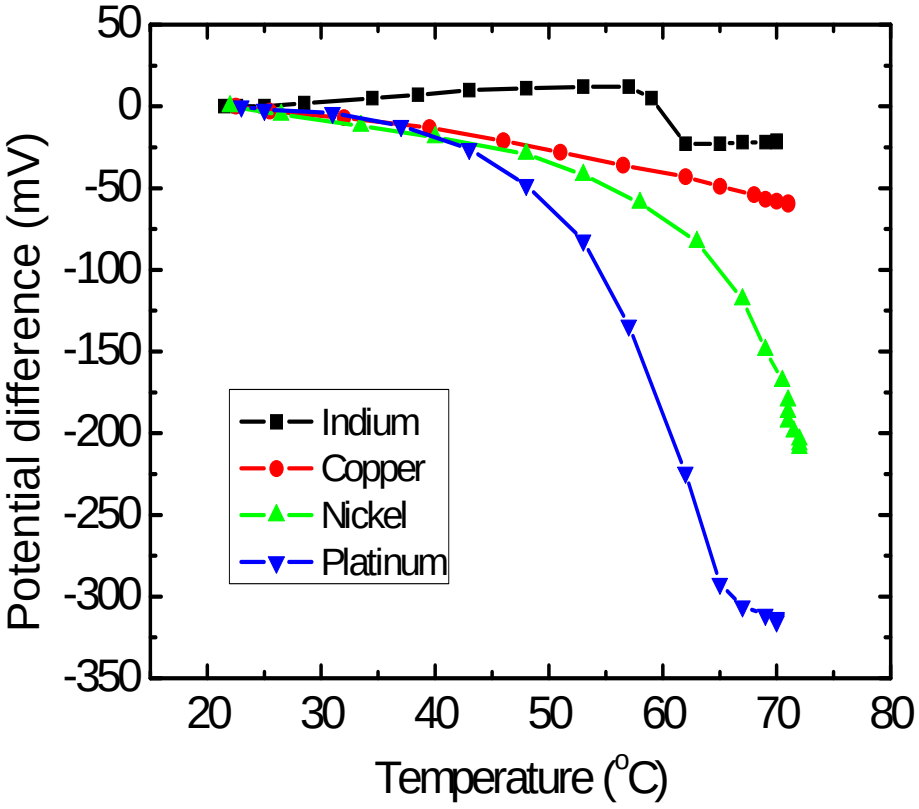

Fig.5.2. Typical results of the output voltage (V) as a function of the temperature difference between the two electrodes (ΔT).

components: One from the Helmholtz layer, C_H, and the other from the diffusion layer, C_D, as depicted by the right-hand side (RHS) of Fig.5.4. While this model is useful to explain many surface phenomena, e.g. the temperature dependence of electrode potential and surface tension, it does not directly capture the influence of the solid phase.

According to the Jellium model [95], a third capacitive component, C_M, should be taken into consideration, which comes from the electron spillover over the electrode surface and can result in an assymetric electron distribution, leading to the formation of a relatively strong dipole moment.

The total capacitance between the bulk liquid phase and the electrode surface (C_{total}) is over all the three capactive components because they are connected in serial; that is

$$C_{total} = \sum \frac{1}{C} = \frac{1}{C_M} + \frac{1}{C_H} + \frac{1}{C_D} \quad (1)$$

The potential difference over the electrical double layer can be determined as ${}^{M}\Delta^{S}\varphi = Q / C_{total}$, where Q is effective surface charge over the electrical double layer. The distribution of the surface charge is determined by the temperature and the electric field within the layer, which can be described by the Poisson-Boltzmann equation [96]. Also, the capacitances in all the regions are changed, because they are dependent on electric field. Here, because the C_H and C_D do not include the metal phase effect in Gouy-Chapman model, it may be reasonable to look into only the change in the C_M when the electrode phase varies, and the variations in C_H and C_D are secondary. The metal

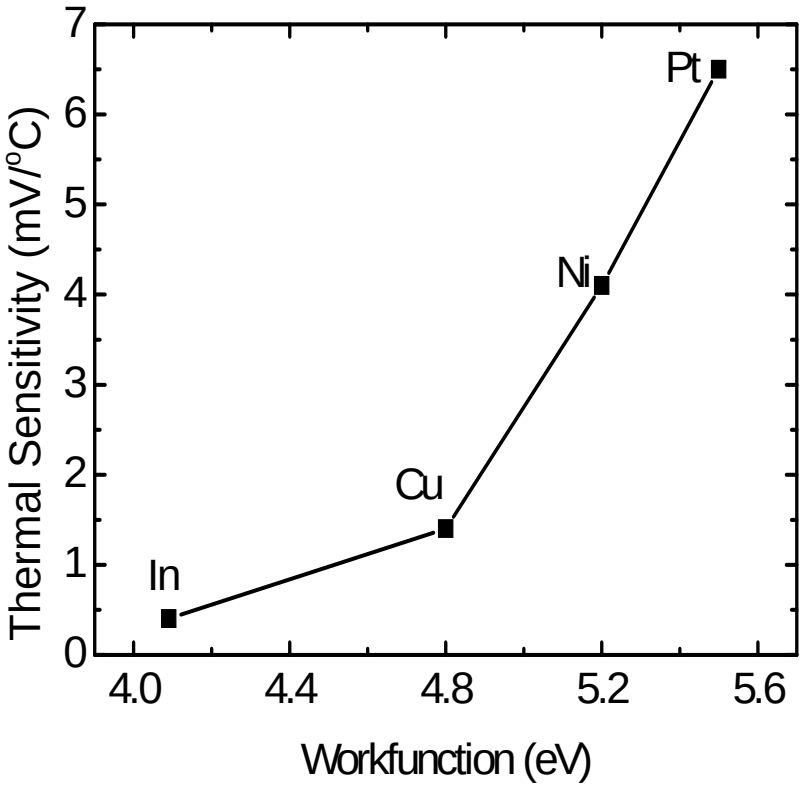

Fig.5.3. The temperature sensitivity of electrode potential (dV/dT) as a function of the work function (ϕ_w).

contribution to the change in the potential difference related to the temperature variation can be written,

$$\frac{\mathrm{d}({}^{\mathrm{M}}\Delta^{\mathrm{S}}\varphi)_{\mathrm{M}}}{\mathrm{dT}} = \frac{d}{dT}\left(\frac{Q}{\mathrm{C_M}}\right) = \frac{1}{\mathrm{C_M}}\left\{\frac{dQ}{dT} - ({}^{\mathrm{M}}\Delta^{\mathrm{S}}\varphi)_{\mathrm{M}} \cdot \frac{d\mathrm{C_M}}{dT}\right\} \sim \frac{1}{\mathrm{C_M}} \cdot \frac{dQ}{dT} \quad (2)$$

where in the above equation the second term can be ignored, because the temperature dependence of the C_M is trivial above room temeprature. [95,97] From Eq.(2), it can be seen that, the derivative of the potential difference with respect to temeperature change is proportional to the term, $1/C_M$.

The Jellium model describes the contribution of the electrode phase to the overall capacitance of the double layer [95], in which C_M is highly dependent on the bulk electron density in the electrode (n_+):

$$\frac{1}{C_M} = -\frac{8\pi n_+ e_0}{\alpha^3}\frac{\partial\alpha}{\partial Q} \quad (3)$$

where α, e_0, and Q are semi-empirical parameters capturing the effects of the electronic density profile, the electronic charge, and the surface charge density, respectively. From Eqs.(2) and (3), it can be derived that the partial potential change is proportional to the bulk electron density (n_+), which is correlated to the work function [98]: A metallic material that has a high n_+ value usually also has a high WF value.

The four electrode materials under investigation have quite different work functions [93], among which In has the smallest WF. According to Fig.5.2, when temperature changes significantly by nearly 50 ^{o}C, the measured electrode potential of In is quite random, probably reflecting the drifting of the internal grounding. The average temperature sensitivity (dV/dT) is only 0.4mV/K, as shown in Fig.5.3. When the electrode material is chagned to Cu, the WF value increases to 4.8eV, and the

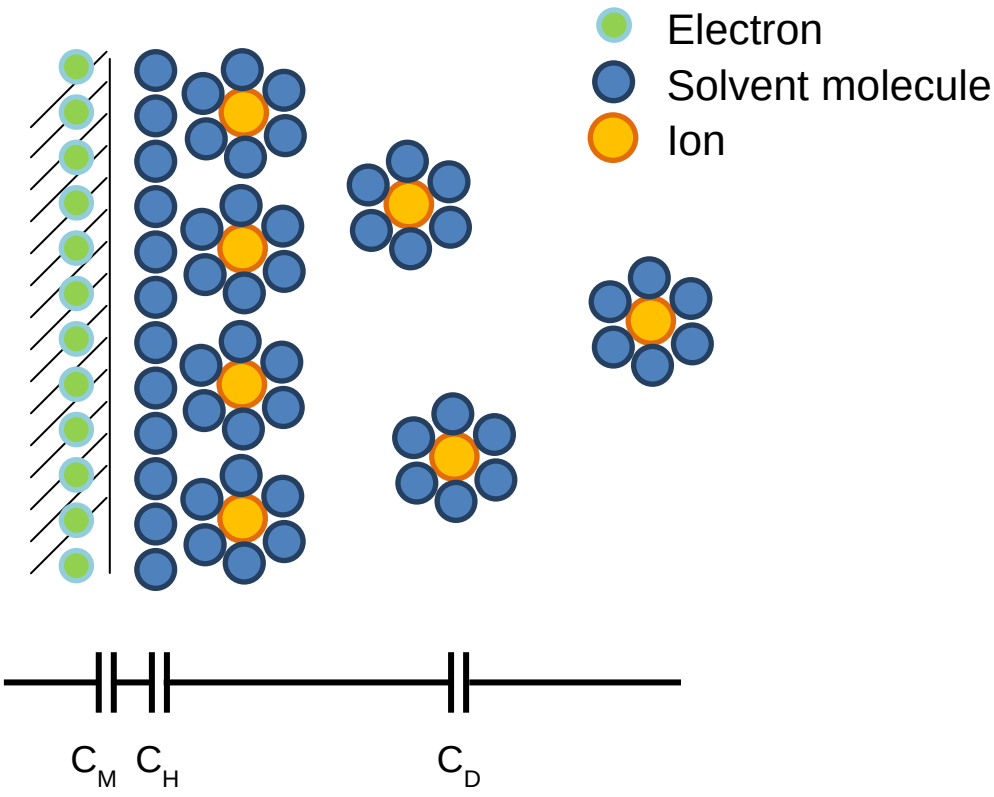

Fig.5.4. Schematic of the surface ion structure.

electrode potential increases monotonically with the temperature. The average temperature sensitivity is 1.4mV/K. For Ni and Pt, the WF values are even much higher, and dV/dT are 4.1mV/K and 6.5mV/K, respectively, both higher than that of Cu. It is clear that dV/dT is positively correlated to WF, fitting well with the prediction of the Jellium model.

Note that except for In, for which the voltage change is qutie small and the measurement results are governed by data scatter, for the rest of the three electrodematerials (Cu, Ni, and Pt) the value of dV/dT is relatively linear to the value of WF, suggesting that the first order approximation used in the above analysis is quite plausible.

Figure 5.2 also shows that the temperature dependence of electrode potential is nonlienar. For Cu, Ni, and Pt, the increase in electrode potential is relatively slow when the temperature is relatively low, and V rises increasingly fast as the temperature becomes higher. The change in electrode potential is related to the variation in the effective adsorption coverage, which can be promoted as T is higher [91].

5.4. Concluding Remarks

In summary, as temperature changes, due to the associated charge motion (ΔQ), the potential difference across the double layer of an electrode-electrolyte interface would vary. The temperature sensitivity of electrode potential is higher if the electrode material has a higher work function, which is of a beneficial effect to the TCS performance. This effect can be explained quite well by the Jellium model, having

important relevance to the optimization of the electrode phase in TCS for harvesting and storing LGH.

CHAPTER 6. Performance of Thermally-Chargeable Supercapacitors in Various Solvents

6.1. Introduction

Low-grade heat (LGH) is one of important energy sources that currently cannot be fully utilized. Usually, LGH is referred to as the thermal energy of heat sources of relatively low temperatures (< 250 ^{o}C) [58]. An example of LGH source is the wasted heat in power generation plants, which is as much as hundreds of Giga-Watt in the U.S. [59]. Other examples include geo-thermal energy, ocean thermal energy, distributed solar thermal energy, etc. [99]. If the energy from these LGH sources can be harvested and stored as electric energy with high energetic and cost efficiency, significant additional "green" power can be generated.

However, the low temperature associated with the LGH makes its harvesting and storage prohibitively difficult by using conventional thermal-to-electric energy conversion (TEEC) techniques. Particularly, the cost and energetic efficiencies of available TEEC methods are quite low for LGH. The major issue for the indirect TEEC procedures is the high installation, operational, and maintenance costs. As any energy conversion process, the upper limit of the energetic efficiency of LGH harvesting is determined by the Carnot cycle limit: $\zeta_c = \Delta T/T$, where T is the LGH temperature and ΔT is the temperature difference between T and the reference temperature (T_r). For a high-temperature heat source, due to the large temperature difference, the Carnot cycle limit is quite high, so that the overall TEEC efficiency $\zeta = \zeta_c \cdot \zeta_m$ may be sufficient to cover the high costs related to the expensive components such as pumps and heat

exchangers as well as the large number of moving parts. Here, ζ_m indicates the machine efficiency. For LGH, while the system costs are similar, the efficiency of energy harvesting (ζ) considerably decreases, resulting in a poor cost-performance balance, typically around a few U.S. dollars per Watt [80], which is non-competitive compared with the grid power.

For the direct, Seebeck effect based TEEC procedures, the key challenges imposed by LGH are associated with the low energy density and the poor energetic efficiency [100]. The low energetic efficiency is caused by both the low Carnot cycle limit and the thermal shorting effect [64]; i.e. as electrons diffuse from the heat source to the heat sink, electric energy generation and thermal energy conduction take place simultaneously, and the thermal energy involved in the latter is essentially wasted. As a result, the cost of harvested energy is often even higher than that of the indirect procedures. In order to utilize the LGH, novel TEEC methods must be developed.

In a recent experiment on thermally dependent capacitive effect [6], we investigated the concept of thermally-chargeable supercapacitors (TCS). As depicted in Fig.6.1, a possible structure of TCS consists of two half-capacitors placed at different temperatures. Each half-capacitor is formed by immersing an electrode in an electrolyte solution. At the electrode-liquid interface, as solvated ions are adsorbed by the solid surface, an ionic double-layer structure would be formed [83], which induces counter charges in the electrode surface, accompanied by the development of an electrode potential, i.e. the potential difference normal to the interface. This capacitive effect is dependent on temperature. When temperature changes, as the adsorption coverage becomes difference, the electrode potential varies. Thus, as the two half-capacitors are

connected, a net output voltage can be produced. The generated electric energy is converted from the consumed thermal energy, and this process can be greatly promoted if large-surface-area, nanostructured electrodes are employed. The preliminary testing data showed that the TCS works well for LGH, since the electrode potential is most thermally sensitive in the low temperature range. The energy density of a TCS can be on the scale of 10^2 mJ/g with a relatively small $\Delta T \sim 50\ ^{o}C$ [83], much higher than that of thermoelectric materials.

One of the key factors dominating the TCS performance is the output voltage, V, the different between the electrode potentials of the two half-capacitors. With everything else being the same, the energy density of the system is proportional to V^2. Since usually the reference temperature (T_r) is kept constant, with a give temperature difference, the value of V is governed by the thermal sensitivity of the electrode potential of the high-temperature half-capacitor, $dV/dT = d\phi/dT$, where ϕ is the electrode potential. The magnitude of dV/dT is related to a number of factors, such as the electrode material, the surface properties, the ion charge/size/concentration, as well as the solvent properties. In the current study, the investigation is focused on the solvent effects.

6.2. Experimental

For the reasons that will be discussed in the next section, we investigated three different solvents: dimethyl sulfoxide (DMSO), water, and formamide (FA). Two types of TCS electrodes were analyzed. The first was platinum (Pt) foil. Each foil was 100μm thick, with the size of 10 mm × 10 mm. They were separately placed in two

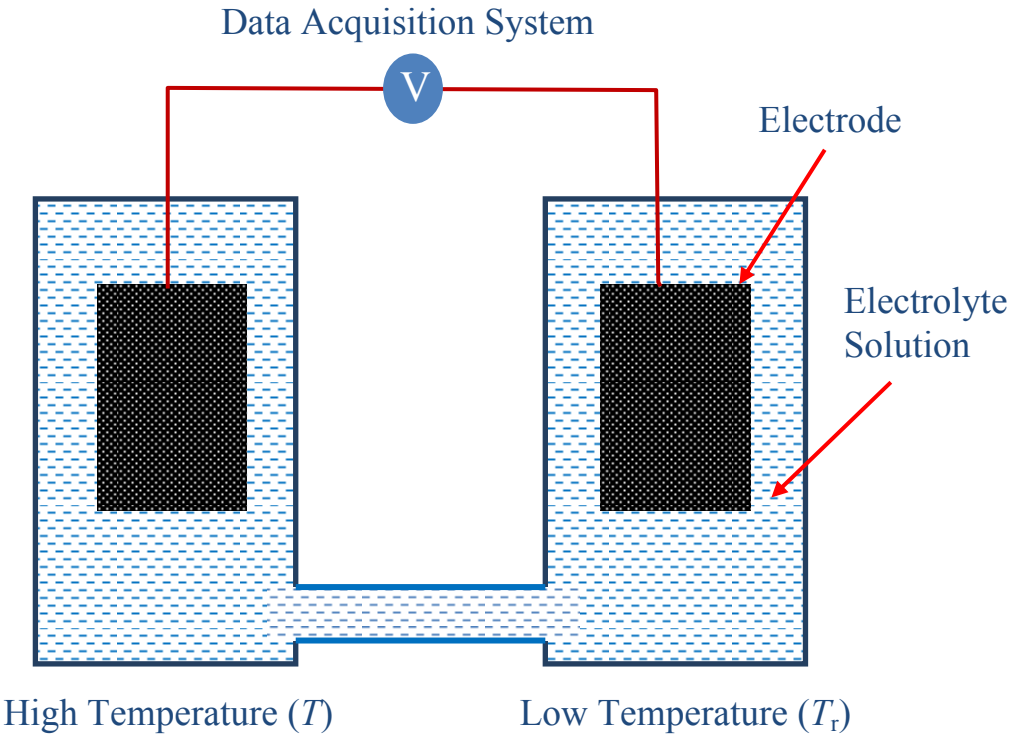

Fig.6.1. Schematic of the experimental setup.

polypropylene (PP) containers, as depicted in Fig.6.1. Each container contained 50 ml of 1 M lithium chloride (LiCl) solution. The liquid phases in the two containers were connected by a salt bridge, which was 5 mm in diameter and 30 mm long. The salt bridge was employed to simplify the system structure. It could actually be replaced by internal grounding with counter electrodes [19]. The two electrodes were connected to a National Instrument SCB-68 Data Acquisition (DAQ) system through Pt wires, so that the voltage between them was monitored continuously.

Initially, both containers were kept at room temperature, 23 ^{o}C. By using a corning PC-220 Hot Plate, one of the containers was heated to 63 ^{o}C, with a constant temperature increase rate of 3 ^{o}C/min. The temperature was measured by type-K thermocouples through an Omega HH-20A Reader. Figure 6.2(a) shows the measured V as a function of temperature increase. The average thermal sensitivity of electrode potential, dV/dT, was calculated as $\Delta V/\Delta T$, where ΔV is the output voltage when the temperature difference $\Delta T = 40$ ^{o}C, as shown in Fig.6.3.

The second type of electrode under investigation was a nanoporous carbon (NC) obtained from Cabot (Product No.: BP2000). The as-received material was in powder form. By using a Micromeritics TriStar-3000 Gas Adsorption Analyzer, the main modal value of pore size distribution was determined as ~3 nm. The specific surface area was 1810 m^2/g. The particle size ranged from a few microns to a few tens of microns. The material was refluxed in neat aceton at 80 ^{o}C for 4 h in a vertical tower, and then filtered and repeatedly rinsed by warm water and methanol. By using a type 5580 Instron machine, about 200 mg of the treated NC particles were pressurized into a thin disk, with the diameter around 5 mm and the thickness around 1 mm. The compression

pressure was 40 MPa and the compression time was sufficient to reach the stable structure. Two NC disks were used in the thermal sensitivity measurement experiment, replacing the two Pt electrodes in the first testing setup, respectively. The measurement procedure was similar to that of the Pt based system. The experimental data of the output voltage are shown in Fig.6.2(b).

6.3. Results and Discussion

The working mechanism of TCS is based on the capacitive effect. As the electrode is immersed in the electrolyte solution, at the solid-liquid interface there would be a high-ion-density zone, where the structure of the solvated ions is double-layered. The effective surface ion density is much higher than that in the bulk liquid phase. As a result, counter charges are induced in the electrode surface, generating electrode potential, ϕ, normal to the interface. As temperature changes, due to the thermally dependent surface ion density and motion, the electrode potential would vary. Thus, as the two electrodes in a TCS that are of different temperatures are connected, a net output voltage, V, can be measured. The associated electric energy is harvested from the thermal energy. Such a system works best in the LGH temperature range, in which the solid-liquid interface is stable and thermally sensitive.

The variation in the potential difference between the electrode phase and the bulk liquid phase can be stated as $\Delta\phi = \Delta(Q/C)$, where Q is the effective surface charge density and C is the effective surface capacitance, and "Δ" indicates the thermally induced change. In an electrolyte solution, a solid-liquid interface consists of a few capacitive components: C_M that captures the contribution of the electrode at the Jellium

edge, C_H that reflects the solvent contribution in the Helmholtz layer, and C_{DL} that is related to the diffuse layer. The potential difference between the electrode phase and the bulk liquid phase can be written as $\Delta\phi = \Delta Q \cdot (1/\Delta C_M + 1/\Delta C_H + 1/\Delta C_{DL})$ [9]. All the three terms at the right-hand side (RHS) are thermally dependent, among which C_M is related to only the electrode phase while C_H and C_{DL} are dependent on the solvent properties. [82] According to Trasatti [101], the potential of the electrode phase at the potential of zero charge (PZC) state shows a strong dependence on the temperature variation. Under the PZC condition, the contributions from the charges in the electrode or the liquid are trivial. The thermal sensitivities of surface potential (dg^S_{dipole}/dT) are -1.15 mV/^{o}C, -1.23 mV/^{o}C and -1.66 mV/^{o}C for DMSO, water, and FA, respectively. From Figs.6.2(a) and 6.3, it can be seen that the thermal sensitivity of output potential of the three solvents are indeed different. The average values of dV/dT are -5.4 mV/^{o}C, -1.0 mV/^{o}C, and -0.3 mV/^{o}C for FA, water, and DMSO, respectively. The trend of the Trasatti's result quantitatively fits with the experimental data, while is much weaker.

The difference between them may come from the influence of the adsorbed ions in the surface double layer. Since the capacitance associated with specifically adsorbed ions (C_{ads}) is the smaller compared with other capacitive components [102], it has dominant effect on the overall surface capacitance, C_{tot}. In a solution of a relatively high ion concentration, the degree of adsorption is significant, as reported in [103] that chlorine ions can generate an unusually large potential difference; e.g. the electrode potential can change by as much as 100 mV with a variation in the effective surface ion density of 2 $\mu C/cm^2$. Under this condition, C_M and C_{ads} are much smaller than C_H and

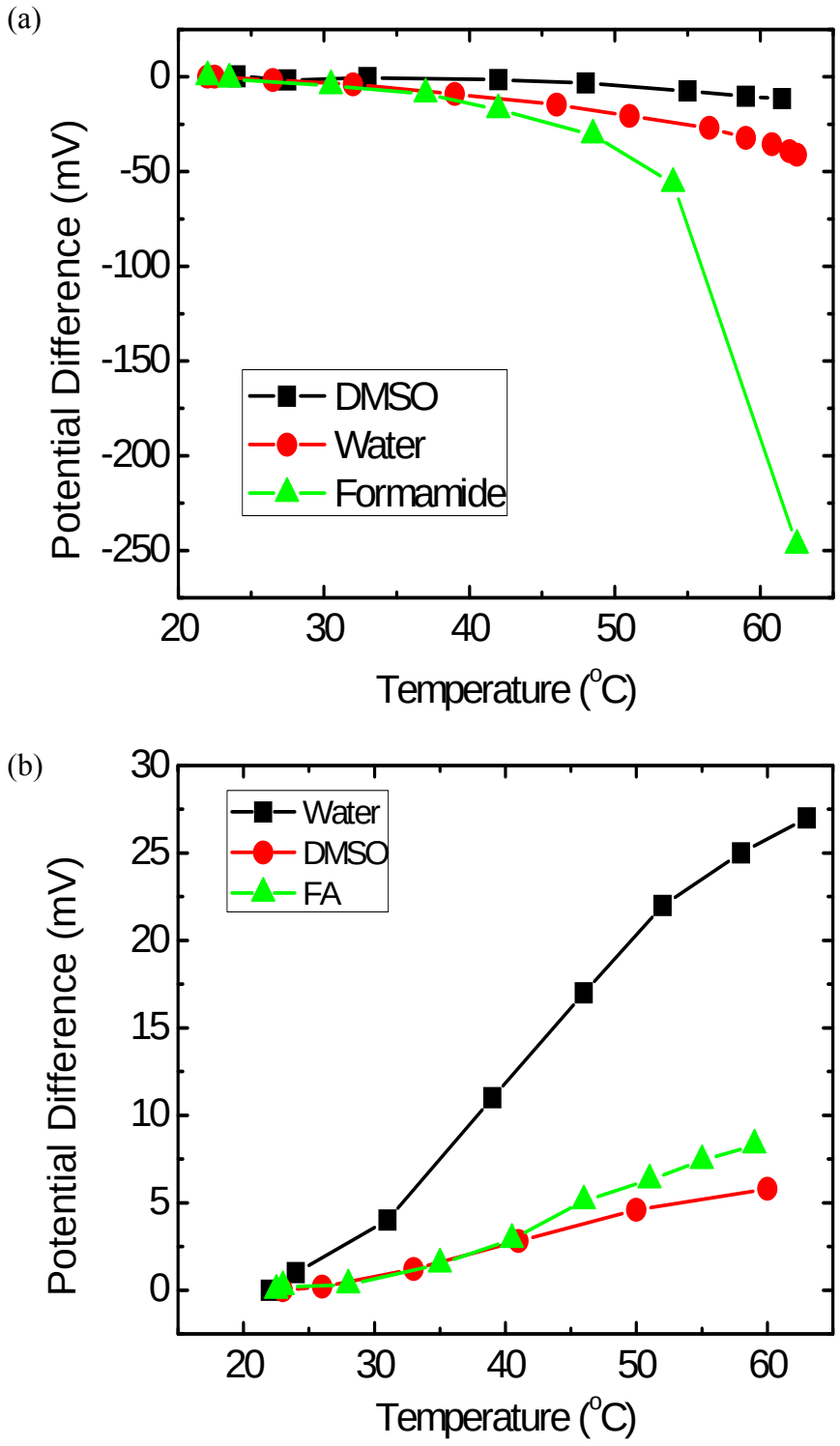

Fig.6.2. Typical measurement results of the output voltage (V) as a function of the LGH temperature (T): (a) Pt electrode; (b) nanoporous carbonelectrode.

C_D, and $\Delta\phi$ should be expressed as $\Delta\phi = \Delta Q \cdot (1/\Delta C_M + 1/\Delta C_{ads})$. As the solvent changes, the degree of adsorption becomes different. The adsorption process consists of three steps: removal of the solvation shell, removal of the solvent layer on the electrode surface, and the adsorption procedure. There is a certain free energy change associated with each step, and the overall system free energy is lowered after the adsorption process is completed. Usually, a solvent of a higher dielectric constant has higher solvating ability. That is, in such a solvent the ions tend to stay in the solvated state, so that the adsorption is relatively difficult. For the solvents under investigation, FA has the highest dielectric constant and DMSO has the lowest dielectric constant. Therefore, on the electrode surface, FA tends to have the lowest degree of adsorption and DMSO tends to have the highest degree of adsorption. A low degree high thermal sensitivity of electrode potential, promoting the surface potential effect.

While the classic surface theory explains well the measured dV/dT data of Pt electrode, according to Fig.6.2(b), the solvent effects for the NC electrode based system are entirely different. For water, FA, and DMSO, the thermal sensitivity of output voltage is 0.68 mV/^{o}C, 0.23 mV/^{o}C, and 0.15 mV/^{o}C, respectively. First, the output voltage, i.e. the electrode potential of the high-temperature electrode, is positively correlated with temperature, T. Second, there is no clear pattern of the relationship between the magnitude of dV/dT and the surface potential and/or the dielectric constant of the solvent.

Both of the characteristics are contradictory to the above discussion and should be related to the confinement effects of nanopore walls. In the NC electrode, the majority of the solid-liquid interface is in the smallest nanopores of the nanopore size

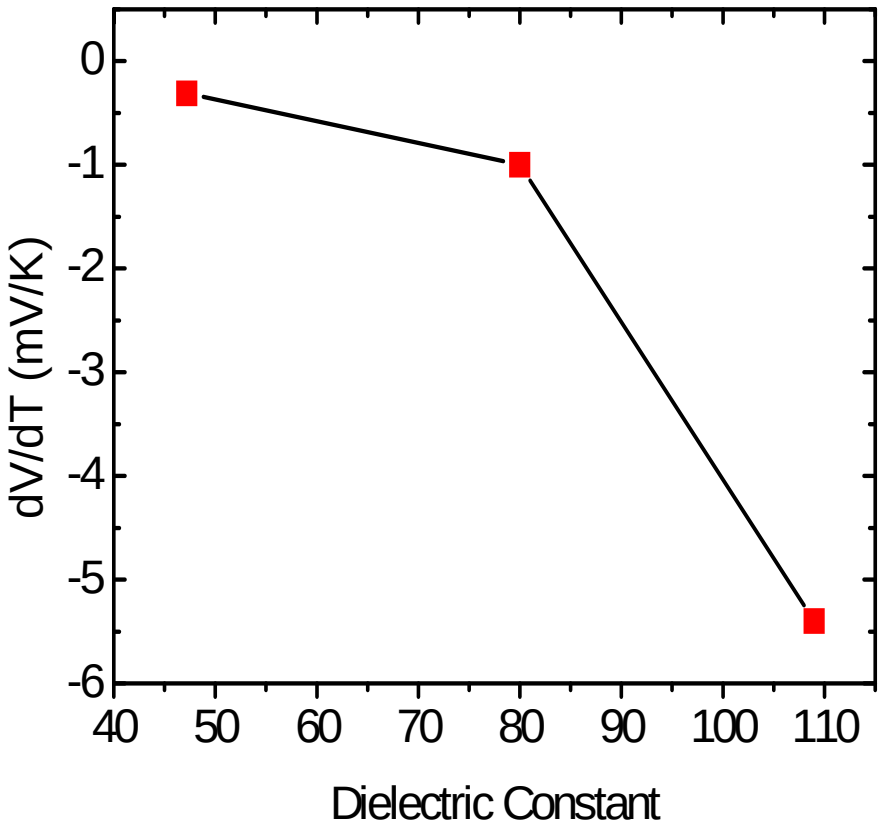

Fig.6.3. The temperature sensitivity of zeta potential (d*V*/d*T*) as a function of the dielectric constant of the solvent. The data are for the Pt-electrode system.

ranging from 1 to a few nm. On such a small length scale, the solvated structure can be distorted, and, therefore, the free energy change associated with the removal of hydration shell can be different from that at a large solid surface, and the influence of solvent molecules on the degree of adsorption tends to be distinct. Furthermore, the surface ion structure is strongly affected by the nanopore surfaces, and the double layer structure may break down [104]. In the smallest nanopores, the entered confined liquid phase is exposed to the solid atoms, and the concept of surface zone must be redefined [e.g. 74]. Probably more importantly, in a nanopore, the thermally driven ion motion can be quite unique. Due to the ultrahigh surface to volume ratio, the liquid in the interior may not be regarded as a bulk phase, and the dominant ion motion should be along the axial direction, which has a different time scale compared with the ion diffusion normal to the solid-liquid interface. In the confining nano-environment, the molecular size of solvent becomes critical. The sizes of water, DMSO, and FA molecules are 0.25 nm, 0.47 nm, and 0.62 nm, respectively. Thus, as a first order approximation, the sizes of solvated lithium cation are 0.65 nm, 1.09 nm, and 1.39 nm for the three solvents, respectively. While for water the smallest nanopores provide a barely enough space to form the Helmholtz layer, for DMSO and FA the space is insufficient. Consequently, the ion motion in DMSO and FA is highly suppressed, leading to the much reduced thermal sensitivity.

6.4. Concluding Remarks

In summary, through an experimental study, it was confirmed that for a large electrode conventional surface theory explains quite well the solvent effects on the

output voltage of a thermally chargeable supercapacitor, based on the analyses on surface potential and dielectric constant. However, when the electrodes are nanoporous, the conventional theory breaks down, which must be attributed to the strong confinement effects of nanopore walls on the sovlated-ion motion. The details of the thermally driven behaviors of confined ions are still under investigation.

CHAPTER 7. Using Thermally-Chargeable Supercapacitor for Fluctuating Low-Grade Heat Sources

7.1. Introduction

Low-grade heat (LGH) is defined as the thermal energy associated with relatively low temperatures (< 250 ^{o}C) [58]. It is ample in nature and in industry. For instance, in the U.S. alone, hundreds of Giga-Watt of LGH is wasted in the cooling systems in coal and nuclear power generation plants [59]. For another example, if the wasted heat in vehicle engines can be harvested and utilized with a high cost and energetic efficiency, the fuel efficiency of the vehicles can be considerably enhanced [105]. Other examples of LGH include solar thermal energy, which accounts for up to 84% of the total energy received by today's solar panels and is being wasted [89,106]; geo/ocean-thermal energy, which currently has only a limited market size due to the lack of cost-efficient energy harvesting and storage techniques [107]; and our body temperature, which may be utilized for self-powered bio-devices; among others.

In the past, LGH harvesting and storage was achieved either through indirect thermal-to-electric energy conversion (TEEC) techniques using turbine engines or Organic Rankin Cycle (ORC) machines [62], or through direct TEEC techniques using thermoelectric materials [108]. In both methods, the TEEC system works in between a high-temperature side (the heat source) and a low-temperature side (the heat sink); i.e. a temperature gradient, usually constant, must be maintained during the TEEC process. The heat source triggers physical processes that are both thermally and electrically related, such as the phase transformation in an ORC machine or the thermally driven

electron diffusion in a thermoelectric material, converting a portion of the consumed thermal energy to electric energy.

The major issues of the conventional TEEC techniques of LGH include the low energy density and the low energetic efficiency, both leading to the poor cost-performance balance. For instance, in a thermoelectric material, as the electrons diffuse from the high-temperature heat source to the low-temperature heat sink, thermal conduction also takes place. Such a phenomenon, often referred to as the thermal shorting effect, causes a relatively low system efficiency (ζ_s), often < 10% for LGH [65]. Due to the low temperature of LGH, the Carnot cycle efficiency $\zeta_c = \Delta T/T$ is also low, where ΔT is the temperature difference between the heat source (T) and the heat sink (T_r). Thus, the overall energetic efficiency of the TEEC system, $\zeta = \zeta_c \cdot \zeta_s$, is usually insufficient to cover the relatively high material cost. For the indirect TEEC systems such as the ORC machines, the high cost comes from the relatively expensive components such as heat exchangers and pumps, as well as the sophisticated installation, operation, and maintenance procedures associated with the large number of moving parts [62]. Usually, the cost of the harvested power from LGH is around a few dollars per Watt [18], much less competitive compared with the grid power.

Another problem of the conventional TEEC techniques is the requirement of the stable temperature gradient. Due to the relatively low energetic efficiency, to generate useful electric energy a relatively large amount of thermal energy must be consumed and dissipated, and, therefore, the heat exchange components are often massive and bulky. Furthermore, for many LGH sources, generating stable temperature gradients may be problematic, such as in a desert area where the temperature field is quite

uniform. Note that the temperatures of some of these LGH sources fluctuate. It is desirable that novel technologies can be developed to harvest and store electric energy from these changing LGH sources, with high energy densities.

7.2. Experimental

Figure 7.1 depicts the experimental setup. The reason why it is so-designed will be discussed in the next section. Figure 7.1(a) depicts a system that works in a constant temperature gradient, and Fig.7.1(b) shows its counterpart that work with temperature fluctuation. In Fig.7.1(b), one electrode and one counter-electrode were immersed in 50 ml of 1 M aqueous solution of sodium chloride (NaCl), sealed in a polypropylene (PP) container.

The electrode was prepared by using Cabot BP2000 nanoporous carbon (NC). The as-received NC was in powder form. It was refluxed in aceton at 80 ^{o}C for 4 h in a vertical tower, and then vacuum dried in a VWR 1410 vacuum oven at 80 ^{o}C for 10 h. About 10 mg of the treated NC powders were firmly compressed into a conductive disk on a 0.1mm thick platinum (Pt) sheet, by using a type 5580 Instron machine. The compression pressure was 40 MPa and the compression time was 5 minutes. The size of the Pt sheet was about 10 mm by 10 mm.

The counter-electrode was made of a multiwall carbon nanotube (MWCNT) obtained from cheaptubes.com, with the product number of sku-030102. The material was refluxed in an acidic solution that contained 1 part of nitric acid (HNO_3) and 3 parts of sulfuric acid (H_2SO_4) at 140 ^{o}C for 4 h. After filtering and repeated cleaning with

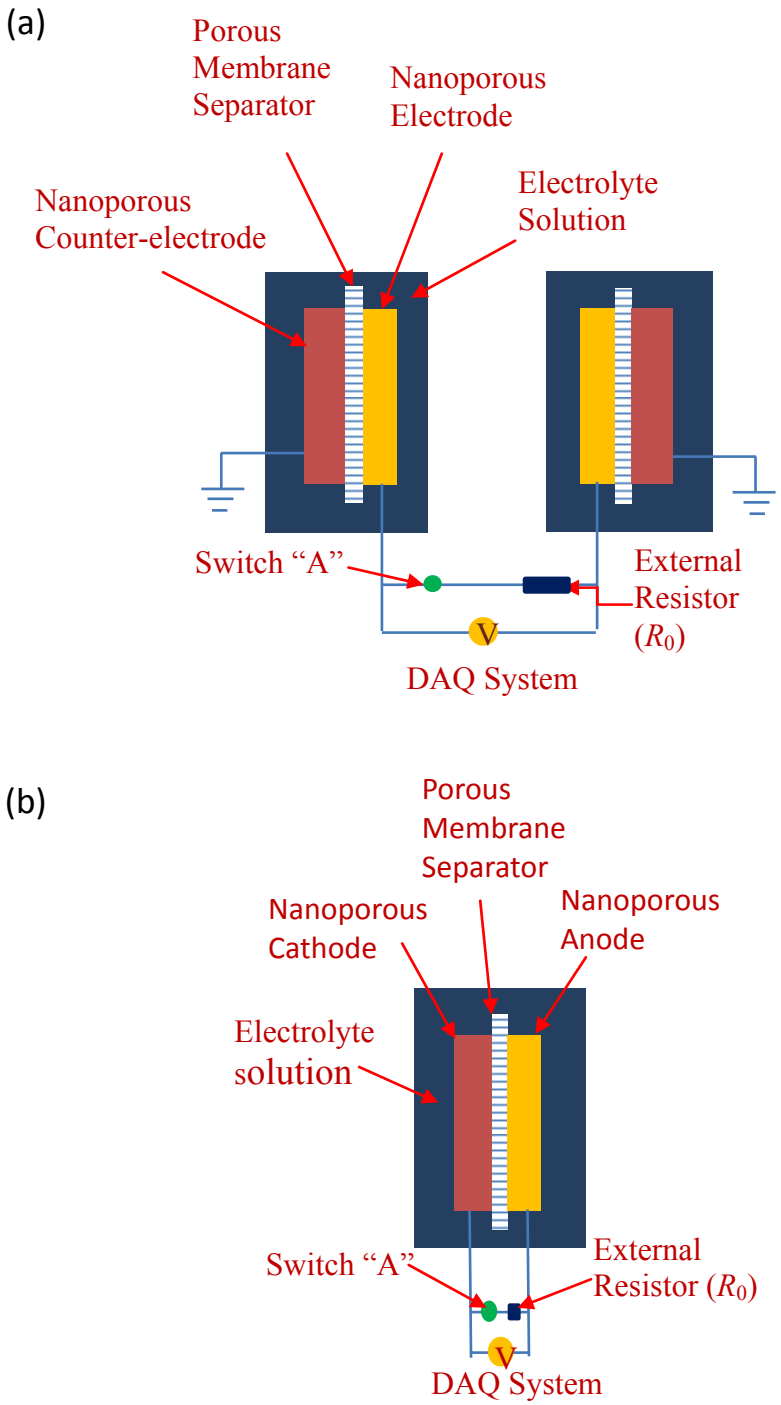

Fig.7.1. Schematics of TCS systems working with (a) a temperature gradient and (b) temperature fluctuation.

water and acetone, 10 mg of the treated CNT was firmly compressed into a disk on a Pt sheet that 0.1mm thick and 10 mm by 10 mm large. The compression was performed by a type 5580 Instron machine, with the pressure of 40 MPa and the compression time of 5 minutes.

The electrode and the counter-electrode was sandwiched with a 25 μm thick celgard 3501 porous membrane separator, and placed at the center of the PP container, immersed in the electrolyte solution. The two Pt sheets, serving as the charge collectors, were connected through switch "A" and an external resistor (R_0), 200 Ω for the cell with NaCl solution and 300Ω for the NaI cell. At room temperature (T_r), switch "A" was turned on for 20 min, until the potential difference between the electrode and the counter-electrode converged to zero. The output voltage (V) was measured by a National Instrument SCB68 Data Acquisition (DAQ) system. Then, switch "A" was turned off and the temperature of the system (T) was raised at the rate of 3 ^{o}C/min, by using a Corning PC-220 Hot Plate. The temperature was monitored by type-K thermocouples equipped with a Omega HH-20A Reader. The open-circuit output voltage was plotted as a function of the system temperature, T, in Fig.7.2.

We performed two experimental sets with different electrolyte and different temperature range to get higher output voltage. For the first testing cell, the electrolyte was 1M of sodium chloride (NaCl) and when the system temperature was increased by 42 ^{o}C higher than the room temperature, T was maintained constant. For the other one, the electrolyte was 1M of sodium iodide (NaI) and the temperature rose from 5^{o}C by 65 ^{o}C. Switch "A" was turned on again and the discharging curve was measured over the external resistor, as shown in Fig.7.3. After V vanished, the system was cooled down to

room temperature at a constant rate of 5^{o}C, with switch "A" on, returning to the initial system configuration. Altogether 3 temperature fluctuation cycles were tested. The system performance in the second and the third cycles was nearly identical to the first one in the both cells.

7.3. Results and Discussion

Figure 7.1(a) shows a system that we investigated previously [64]. It works in a constant temperature gradient between two identical PP containers. In each container, a NC electrode is immersed in an electrolyte solution. The liquid phases in the two containers are connected through a salt bridge. Initially, the two containers are of the same temperature and the potential difference between them (V) is zero. As one of the containers is kept at constant temperature, T_r, the other one is gradually heated, and a significant output voltage is generated, with the thermal sensitivity of about 0.64 mV/^{o}C.

The output voltage comes from the thermal dependence of electrode potential in the electrolyte solution. When a solid surface is in contact with a liquid phase, due to the difference force fields from both sides of the interface, the surface ion structure becomes double-layered, leading to the formation of compact Helmholtz layer that induce counter charges in the electrode phase [109]. The potential difference between the liquid phase and the solid surface is referred to as the electrode potential. When temperature changes, since difference factors, such as the ion mobility, the effective liquid viscosity, and the potential functions among solid and liquid atoms/molecules and solvated ions, vary with different rates, the electrode potential becomes different. For

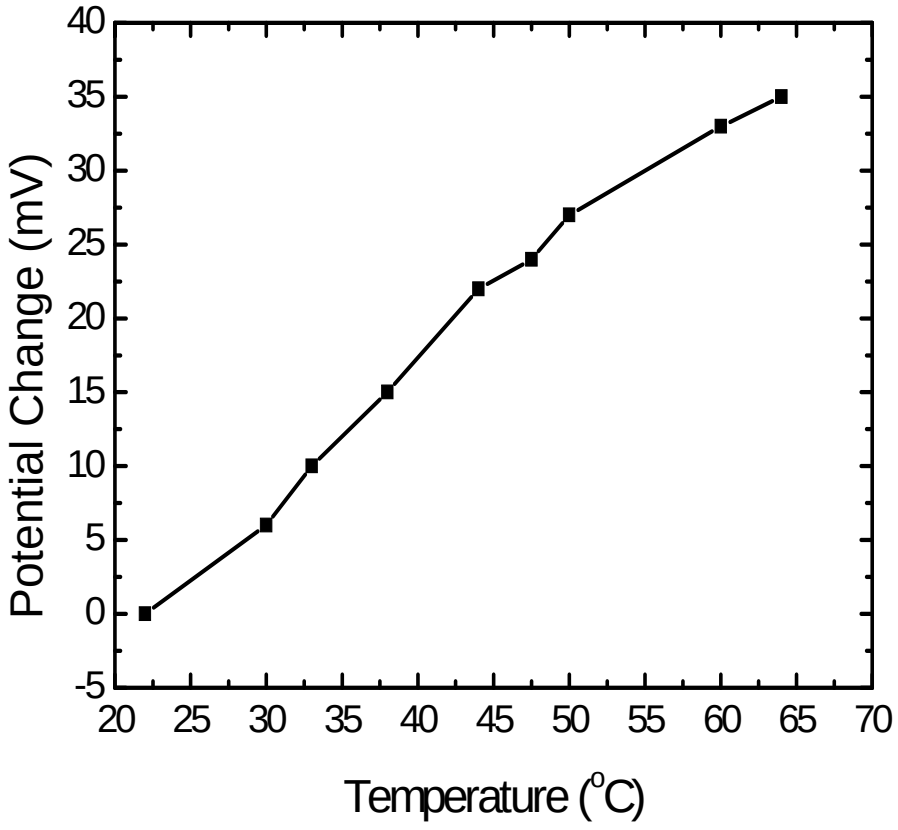

Fig.7.2. Typical measured results of the output voltage as a function of the LGH temperature.

the NC electrode, because the nanopore walls confine the ion motion along the radius direction and the effective time constant of axial ion diffusion is on a different scale, the electrode potential tends to increase with temperature, *T*. As a result, when the high-temperature electrode and the room-temperature one are connected, a certain amount of thermal energy can be converted to electric energy, which is amplified by the large surface area of the NC disk (~10^3 m^2/g). During this process, the heat source does not change.

In the current experimental setup, two nanostructured electrodes are used. The NC electrode is similar with the one discussed above, and the counter-electrode is surface-conditioned CNT bundle. The surface conditioning treatment activates the surface hydroxyl and carboxylic functional groups. They are separated by the porous membrane separator, so that electric shorting is prevented. At room temperature, such a structure is essentially a double-layer supercapacitor (DLS). If a voltage is applied across the electrode and the counter-electrode, a large amount of electric energy can be stored.

In our test, no external electric power source is involved. The two materials are of different electrode potentials. When switch "A" is turned on, a transient current is generated, until a new equilibrium condition is reached, at which the net output voltage between the two electrodes is zero. This is the initial condition of the TEEC procedure.

When temperature, *T*, rises, the electrode potentials of the electrode and the counter-electrode vary. The temperature sensitivity of the electrode potential (dV/dT) of the NC electrode in 1M NaCl solution is the same as that in the two-cell test, ~ 0.64

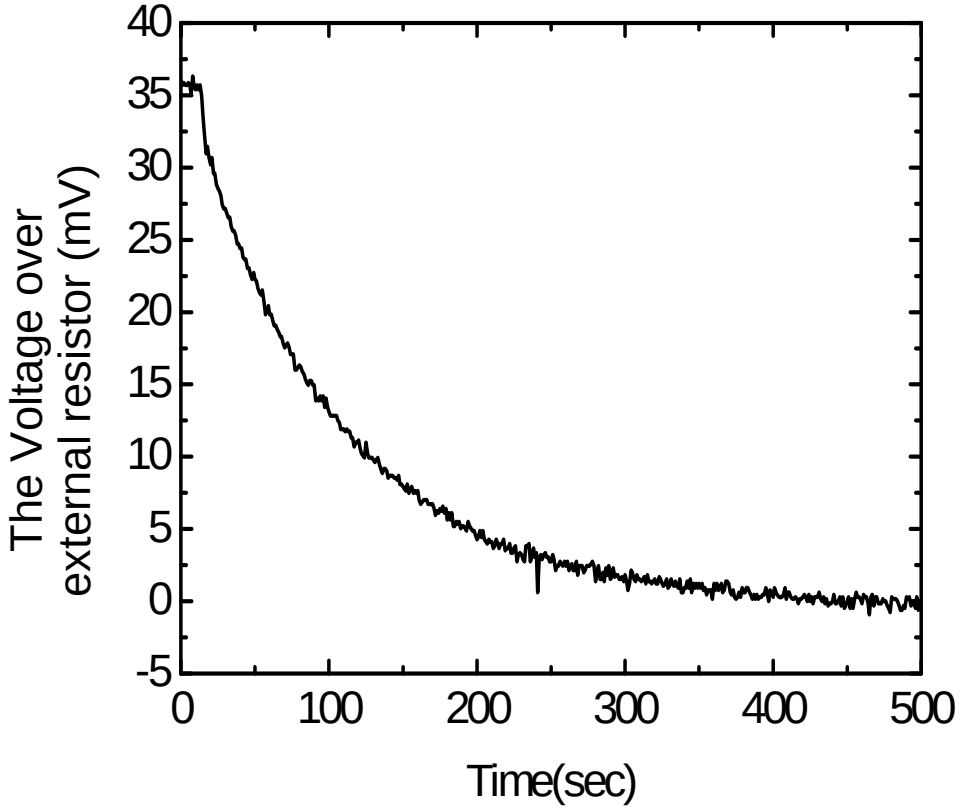

Fig.7.3. A typical discharging curve

mV/^{o}C. The temperature sensitivity of the electrode potential of the counter electrode in the same soltuion is of a much smaller magnitude and an opposite sign, ~ -0.09 mV/^{o}C. As switch "A" is turned off, the potential difference between the two electrodes increases monotonously with T, with a rate of 0.83 mV/^{o}C (Fig.7.2), the same as the summation of the thermal sensitivities of the two electrodes, as it should be. For the second test with NaI solution, the overall temperature sensitivity the cell was 0.92 mV/^{o}C. The difference in the dV/dT between the both tests came from the difference anion. [72]

The thermal sensitivity of electrode potential of a material is determined by a large number of factors, including the work function of electrode, the surface properties, the ion concentration, the ion charge, the ion size, the nanoenvironment, etc. For the current system, the liquid phase for the electrode and the counter-electrode is identical. The difference in dV/dT must come from the solid phase. For instance, in the NC electrode, the solvated ions are confined in the nanopores. Based on the gas absorption analysis result [110], the nanopore size distribution is bimodal, with the peak value contributing most to the specific surface area around 2-3 nm. In such small nanopores, no bulk liquid phase can exist and the ion diffusion must be along the axial direction. In the CNT counter-electrode, while the surfaces are nanostructured, the solvated ions are not confined, directly accessible to the surrounding bulk liquid phase. Consequently, not only the magnitude of dV/dT of the two materials are different, but the signs are opposite. The counter-electrode surface is quite polar, and, therefore, the surface ion structure is less sensitive to the temperature change. With a higher T, as the solvated ions are more mobile, the effective adsorption coverage decreases, so does the electrode

potential. In the NC electrode, the confinement effect of nanopore walls is the governing factor, which suppresses the direct ion exchange between the confined liquid phase and the bulk ion reservoir, resulting in the increase in electrode potential as T becomes higher.

At an elevated temperature, as switch "A" is turned on and the two electrodes are connected, a transient current will be generated. Charges move from the high-potential end to the low-potential end, as shown in Fig.7.3. The output electric energy can be calculated as $\int V^2/R_0 \mathrm{d}t$, with t indicting time, through which the energy density of the system is determined as 18 mJ per gram of electrode material with NaCl solution and 101mJ per gram with NaI solution. In such a LGH temperature range, this value is much higher than that of thermoelectric materials [49].

When the new equilibrium is established and V vanishes, as switch "A" is kept on, the system temperature is decreased back to the initial point, T_r. During the cooling process, the solvated ions redistribute at the solid surfaces, and return to the initial configuration, ready for the next energy harvesting/storage cycle. As such procedures are repeated, significant electric energy is generated associated with the temperature fluctuation.

7.4. Concluding Remarks

By taking advantage of the difference in thermal sensitivities of electrode potential of a nanoporous carbon (the electrode) and a surface conditioned carbon nanotube bundle (the counter-electrode), a single-cell thermally-chargeable supercapacitor system is developed. It harvests and stores LGH as electric energy as

temperature fluctuates, and does not demand a temperature gradient. With the same temperature change, the output voltage of the single-cell TCS can be higher than that of the two-cell system, as the thermal sensitivities of the electrode and the counter-electrode are of opposite signs. The range of the energy density of the systems under investigation is from 18 mJ/g to 101mJ/g with a relatively small temperature variation of 42^{o}C to 65^{o}C.

CHAPTER 8. Conclusions

To develop advanced energy harvesting systems, a novel concept using nanoporous materials is investigated. We found the working mechanism of our NTEECS, and investigated how to improve its performance in terms of electrode, electrolyte and solvent. Our experimental data have shown encouraging results: the output voltage and the energy conversion efficiency are higher than that of conventional thermoelectric materials by orders of magnitude.

First, the testing data have showed that using different cations can significantly affect the TCS properties. When the cation size increases, with everything else being the same, $|dV/dT|$ decreases. The decrease in $|dV/dT|$ is more pronounced when the cation size is relatively small or large, compared with the intermediate range of d.

Second, temperature rises, the electrode potential of the nanoporous carbon under investigation increases, and its thermal sensitivity ($|dV/dT|$) does not decrease monotonously. These unique phenomena may be related to the lack of bulk phase in the confining nanopore environment.

Third, it is found that anion size has significant effects on the thermal sensitivity of electrode potential. Moreover, $|dV/dT|$ increases with the anion size; that is, with everything else being the same, increasing anion size has a beneficial effect for enhancing the TCS performance.

Fourth, the temperature sensitivity of electrode potential is higher if the electrode material has a higher work function, which is of a beneficial effect to the TCS performance. This effect can be explained quite well by the Jellium model, having

important relevance to the optimization of the electrode phase in TCS for harvesting and storing LGH.

Fifth, it was confirmed that for a large electrode conventional surface theory explains quite well the solvent effects on the output voltage of a thermally chargeable supercapacitor, based on the analyses on surface potential and dielectric constant. However, when the electrodes are nanoporous, the conventional theory breaks down, which must be attributed to the strong confinement effects of nanopore walls on the sovlated-ion motion.

Finally, by taking advantage of the difference in thermal sensitivities of electrode potential of a nanoporous carbon (the electrode) and a surface conditioned carbon nanotube bundle (the counter-electrode), a single-cell thermally-chargeable supercapacitor system is developed. It harvests and stores LGH as electric energy as temperature fluctuates, and does not demand a temperature gradient. With the same temperature change, the output voltage of the single-cell TCS can be higher than that of the two-cell system, as the thermal sensitivities of the electrode and the counter-electrode are of opposite signs. The range of the energy density of the systems under investigation is from 18 mJ/g to 101mJ/g with a relatively small temperature variation of 42^{o}C to 65^{o}C.

For future work, we have much room for improving the performance of the NTEECS, for example, by taking another high surface area electrode with high workfunction, finding new solvents suitable to nanoporous environment and applying the understandings the motion of ions in confined nano-structures. We also expect to develop more optimized cell configuration for practical use.

REFERENCES

[1] T. M. Tritt and M. A. Subramanian, MRS Bulletin.Vol. 31, p. 188 (2006)

[2] M. Kenisarin and K. Mahkamov, Renewable and Sustainable Energy Reviews, Vol. 11(9) pp.1913–1965 (2007)

[3] A. Abhat, Solar Energy, Vol 30(4), p.313-332 (1983)

[4] D. D. Pollock, CRC Handbook of Thermoelectrics, Chapter 2

[5] H. Bottner, G.Chen, and R. Venkatasubramanian, MRS Bulletin,Vol. 31, p. 211 (2006)

[6] A. M. Rao, X. Ji, and T. M. Tritt, MRS Bulletin, Vol. 31, p. 218 (2006)

[7] K. Koumoto, I. Terasaki and R. Funahashi, MRS Bulletin.Vol. 31, p. 206 (2006)

[8] Proceedings of the European Conference on Thermoelectrics, ECT2007, Odessa, Ukraine, (2007)

[9] R. Haase, Thermodynamics of Irreversible Processes, Addison-Wesley, New York, (1969)

[10] T.I. Quickenden and Y.Mua, J. Electrochem. Soc. Vol. 142(11), p. 3985 (1995)

[11] Y.V. Kuzminskii, V.A. Zasukha and G.Y. Kuzminskaya, Journal of Power Source, Vol. 52 (2) , p.231 (1994)

[12] T.I. Quickenden and C.F. Vernon, Solar Energy, Vol. 36 (1), pp 63-72 (1986)

[13] T. Ikeshoji, Bulletin of the Chemical of Japan, Vol. 60, pp1505-1514 (1987)

[14] J.M. Hornut and A. Strock, Journal of Applied Electrochemistry, Vol. 21, pp.1103-1113 (1991)

[15] T.C. Hung,. Energy Conversion and Management, Vol. 42, p.539 (2001)

[16] U. Drescher and D. Briggemann, Applied Thermal Engineering, Vol. 27(1), pp.223-228 (2007)

[17] B. Kongtragool and S. Wongwises, Renewable and Sustainable Energy Reviews, Vol. 7 (2) p.131 (2003)

[18] R. Hu, B.A. Cola, N. Haram, J.N. Barisci, S. Lee, S. Stoughton, G. Wallace, C. Too, M. Thomas, A.Gestos,M.E. Cruz, J.P. Ferraris, A.A. Zakhidov, and R.H. Baughman, Nanoletters, Vol. 10, pp. 838-846 (2010)

[19] H.Lim and Y.Qiao,"Using Thermally-Chargeable Supercapacitor for Fluctuating Low-Grade Heat Sources", to be submitted to Engineering Letters

[20] J. O'M. Bockris, A. K. N. Reddy and M. Gamboa-Aldeco, Modern Electrochemistry 2A, 2nd edition, chapter 6

[21] S. Polarz, B. Smarsly. Journal of Nanoscience & Nanotechnology, Vol. 2, p581 (2002).

[22] B. L. Smith, T. E. Shaffer, M. Viani, J. B. Thompson, N. A. Frederick, J. Kindt, A. Belcher, G. D. Stucky, D. E. Morse and P. K. Hansma, Nature, Vol. 399 (1999), pp. 761–763.

[23] Y. S. Lin, I. Kumakiri, B. N. Nair and H. Alsyouri, Separation and Purification Methods, Vol. 31, p.229 (2002)

[24] J. Hayashi, Y. Watada and K. Muroyama, Materials Letter, Vol. 50, p87 (2001)

[25] R.W. Stout, G.B. Cox and T.J. Odiorne, Chromatographia Vol.24, p601 (1987)

[26] A. Han, Y. Qiao, Chemistry Letters, Vol.36(7) p.882 (2007)

[27] D. W. Deamer, M. Akeson, Trends in Biotechnology, Vol. 18, pp.147–151 (2000)

[28] J. Lee, S. Yoo, T. Hyeon, S. M. Oh and K. Kim, Chemical Communication, Vol. 21, p.2177 (1999)

[29] R. Ryoo, S.H. Joo and S.J. Jun, Physical Chemistry B, Vol. 103, p. 7743 (1999)

[30] S. Jun, S.H. Joo, R. Ryoo, M. Kruk, M. Jaroniec, Z. Liu, T. Ohsuna and O. Terasaki, Journal of American Chemical Society, Vol. 122, p.10712 (2000)

[31] S. Iijima, Nature, Vol 354, pp. 56–58 (1991).

[32] F. Valencia, A.H. Romero, E. Hernandez, M. Terronesand, H. Terrones, New Journal of Physics, Vol.5, pp. 123.1-123.16 (2003)

[33] M. Steinhart, J. H. Wendorff, A. Greiner, R. B. Wehrspohn, K. Nielsch, J. Schilling, J. Choi and U. Gösele, Science, Vol. 296(5575), p.1997 (2002)

[34] D. Kramer, R. N. Viswanath, and J. Weissmüller, Nano Letters, Vol. 4 (5), pp. 793-796 (2004)

[35] J. R. Hayes, A. M. Hodge, J. Biener, A.V. Hamza and K. Sieradzki, Journal of Materials Research, Vol. 21, pp. 2611-2616 (2006)

[36] Y. Qiao, G. Cao, and X. Chen, Journal of American Chemical Society, Vol. 129, p. 2355 (2007)

[37] W. K. Liu, E. G. Karpov, S. Zhang, and H. S. Park, Computer Mothods in Applied Mechanics and Engineering, Vol. 193, p. 1529 (2004)

[38] A. Han, X. Chen, and Y. Qiao, Langmuir, Vol. 24, p. 7044 (2008)

[39] A. Han and Y. Qiao, Langmuir, Vol. 23, p. 11396 (2007)

[40] J. O. Bockris and S. U. M. Khan, Surface Electrochemistry, Springer, New York (1993)

[41] A. Peigney, C. Laurent, E. Flahaut, R. R. Bacsa, A. Rousset, Carbon, Vol. 39, p. 507 (2001)

[42] A. Fujiwara, K. Ishii, H. Suematsu, H. Kataura, Y. Maniwa, S. Suzuki, Y. Achiba, Chemical Physics Letter, Vol. 336, p. 205 (2001)

[43] O. Byl, J. Liu, J. T. Yates, Langmuir, Vol. 21, p. 4200 (2005)

[44] A. Rufer, D. Hotellier and P. Barrade, IEEE Transactions on Power Delivery, Vol. 19 (2), pp. 629-636 (2004)

[45] C.E.D. Chidsey, Science, Vol. 251(4996), pp.919-922 (1991)

[46] S. Yamazaki, A.Takegawa, Y. Kaneko, J. Kadokawa, M. Yamagata, and M. Ishikawa, ECS Transactions, Vol. 25 (33), pp. 107-116 (2010)

[47] H. Lhermet, C. Condemine, M. Plissonnier, R. Salot, P. Audebert, and M. Rosset, IEEE Journal of Solid-state Circuits, Vol. 43(1), p.246 (2008)

[48] L. E. Bell, Science, Vol. 321(5895) pp.1457-1461 (2008)

[49] J. P. Heremans, V. Jovovic, E. S. Toberer, A. Saramat, K. Kurosaki, A. Charoenphakdee, S. Yamanaka, G. J. Snyder, Science, Vol. 321 (5888) pp. 554-557 (2008)

[50] B. Zalba,J.M. Marin, L.F.Cabeza, and H. Mehling, Applied thermal Engineering vol. 23, pp.251-283 (2003)

[51] R. Velraj**,** R. V. Seeniraj**,** B. Hafner**,** C. Faber and K. Schwarzer**,** Solar Energy, Vol. 65 (3), pp.171-180 (1999)

[52] T. C. Hung**,** T. Y. Shai and S. K. Wang, Energy, Vol.22 (7), pp.661-667 (1997)

[53] S. Zhou, X Li, Z Wang, H Guo, W Peng, Transactions of Nonferrous Metals Society of China, Vol. 17 (6), pp. 1328-1333 (2007)

[54] J. O'M. Bockris, A. K. N. Reddy and M. Gamboa-Aldeco, Modern Electrochemistry 2A 2nd edition, chapter 6

[55] J. O'M Bockris, A. K. N. Reddy, and M. Gamboa-Aldeco, Modern electrochemistry 2A-Fundamentals of Electrodics, Chapter 6, p919

[56] J. O'M Bockris, A. K. N. Reddy, and M. Gamboa-Aldeco, Modern electrochemistry 2A-Fundamentals of Electrodics, Chapter 6, p882

[57] A. Frumkin, *Journal of Physical Chemistry, Vol.* 166, p. 466 (1925)

[58] A. Kapil, I. Bulatov, J. Kim, R. Smith, Chemical Engineering Transactions Vol. 21, p.367 (2010)
[59] R. H. Lasseter, P. Paigi, "Microgrid: A Conceptual Solution", 35th Annul IEEE Power Elecrronics Specialisrs Conference (2004)

[60] R.J. Krane, Energy Storage Systems, Kluwer Academic Publishers, Dordrecht, pp. 37–67 (1989)

[61] B. Zalba, J.M. Marin, L.F.Cabeza, and H. Mehling, Applied thermal Engineering vol. 23, pp.251-283 (2003)

[62] E. Barbier, Renewable Sustainable Energy Review, Vol. **6**, pp. 3–65 (2002)

[63] C.E.D. Chidsey, Science, Vol. 251(4996), pp.919-922 (1991)

[64] Y. Qiao, V. K. Punyamurtual, A. Han, H. Lim, Journal of Power Sources,Vol. 183, pp. 403–405 (2008)

[65] I. Sur and A. Casian, Physical Review B, Vol. 69, p. 035306 (2004)

[66] S. S. Zumdahl, S. A. Zumdahl, Chemistry 8th edition, Charles Hartford publishers, Chapter 8

[67] A. J. Bard, L. R. Faulkner, "Electrochemical Methods – Fundamentals and Applications", Chapter 12, pp 566-567

[68] J. O'M Bockris, A. K. N.Reddy, and M. Gamboa-Aldeco, Modern electrochemistry 2A-Fundamentals of Electrodics, Chapter 6, p 872

[69] Y. Huang, Journal of Catalysis, Vol. 25, pp. 131-138 (1972)

[70] A. Frumkin, A.Slygin, Acta Physicochimica. U.R.S.S, Vol. 3, p. 791 (1935)

[71] H. Lim and Y. Qiao, "Effects of Ion Concentration on Thermally-Chargeable Double-Layer Supercapacitors" to be submitted to Appl. Phys. Lett.

[72] H. Lim and Y. Qiao, "Anion Size Effect on Electrode Potential in a Nanoporous Carbon" to be submitted to Appl. Phys. Lett.

[73] J. O'M Bockris, A. K. N. Reddy, and M. Gamboa-Aldeco, Modern electrochemistry, Vol. 2A, 2nd edition, Kluwer Academic Publishers, Chapter 6, p.926

[74] K. Yang, S. Yiacoumi and C. Tsouris, Journal of Chemical Physics, Vol. 117(18), p. 8499 (2002)

[75] Q. Shao, L.L. Huang, J. Zhou, L.H. Lu, L.Z. Zhang, X.H. Lu, S.Y. Jiang, K.E. trGubbins and W.F. Shen, Physical Chemistry Chemical Physic, Vol.10, p.1896 (2008)

[76] H. Kwak and E. F. Hasselbrink Jr., Journal of Colloid and Interface Science, Vol.284 (2), p.753 (2005)

[77] D. Li and H. T. Wang, Journal of Materials Chemistry, Vol. 20, p.4551 (2010).

[78] A. Sharma, V.V. Tyagi, C.R. Chen, D. Buddhi, Renewable and Sustainable Energy Reviews, Vol. 13, pp. 318–345 (2009)

[79] T. Wang, Y. Zhang, Z. Peng and G. Shu, Renewable and Sustainable Energy Reviews, Vol. 15, pp. 2862– 2871(2011)

[80] W. W. Husband and A. Beyene, International Journal of Energy Research, Vol. 32, pp. 1373-1382(2008)

[81] Stone, K.W., C.W. Lopez, and R. McAlister, Proceedings of the IECEC, Atlanta, Georgia (1993).

[82] W. R. Fawcett, Oxford university press, Liquids, Solutions, and Interfaces, Oxford University Press, chapter 10 (2004)

[83] H. Lim and Y. Qiao, "Dependence on Cation Size of Thermally Induced Capacitive Effect of a Nanoporous Carbon" to be submitted to Journal of Materials Research

[84] Shaheen A. Al-Muhtaseb and James A. Ritter, Journal of Physical Chemistry B, Vol. 103, pp. 8104-8115 (1999)

[85] J. O'M Bockris and A.K.N. Reddy, Modern Electrochemistry Vol. 1, 2nd edition, Kluwer Academic Publishers, Chapter 2, p 145

[86] M.D. Levi,S. Sigalov, G. Salitra, D. Aurbach and J. Maier, A Europian Journal of Chemical Physics and Physical Chemistry, Vol. 12 (4). pp. 854-862 (2011)

[87] J. O'M Bockris and A.K.N. Reddy, Modern Electrochemistry Vol. 1, 2nd edition, Kluwer Academic Publishers, Chapter 2, p 110

[88] A. Tanimura, A. Kovalenko and F. Hirata, Langmuir, Vol. 23, p. 1509 (2007)

[89] http://www.kyocerasolar.com/products/ksimodule.html

[90] H. J. Goldsmid and G. **S.** Nola, 20th International Conference on Thermoelectrics (2001)

[91] J. O'M Bockris, A. K.N.Reddy, and M. Gamboa-Aldeco, Modern electrochemistry 2A-Fundamentals of Electrodics, Kluwer Academic/Plenum Publishers, Chapter 6, pp 938-941

[92] J. W. Mayer, S.S. Lau, Electronic Materials Science, Maxwell Macmillan, chapter. 4

[93] L. F. Deis, CRC handbook of Chemistry and Physics 2008-2009, pp12-114

[94] J. O'M. Bockris, A. K. N. Reddy, and M. Gamboa-Aldeco, Modern Electrochemistry Volume 2A, 2nd Edition, Kluwer Academic/Plenum Publishers, chapter 6, p.876

[95] W. Schmickler and D. Henderson, Progress in Surface Science Vol 22(4), pp. 323-420 (1986)

[96] J. O'M. Bockris, Amulya K. N. Reddy, and Maria Gamboa-Aldeco, Modern Electrochemistry Volume 2A, 2nd Edition, Kluwer Academic/Plenum Publishers, chapter 6, p.1000

[97] S. Amokrane and J.P. Badiali J. Electroanal. Chem., 266 pp.21-35 (1989)

[98] W. R. Fawcett, "Liquids, Solutions, and Interfaces", Oxford University Press, chapter 10, p 540

[99] D. Tanner, Renewable Energy, Vol. 6 (3), pp. 367-373 (1995)

[100] M. S. Dresselhaus, G. Chen, M. Y. Tang, R. G. Yang, H. Lee, D. Z. Wang, Z. F. Ren, J. P. Fleurial, and P. Gogna, Materials Research Society Symposium Proceeding, Vol. 886**,** pp.1–10 (2006)

[101] S. Trasatti, Electrochemica Acta, Vol. 32(6), pp. 843-850 (1987)

[102] J. R.Macdonald and C.A. Barlow Jr, The Journal of Chemical Physics,Vol. 36 (11) p.3062 (1962)

[103] R. Payne, Transactions of the Faraday Society, 64, pp 1638-1655 (1968)

[104] K. Yang, T.-Y. Ying, S. Yiacoumi, C. Tsouris, and E. S. Vittoratos, Langmuir Vol. 17, p. 1961 (2001)

[105] K. Smith, M. Thornton, 23rd International Electric Vehicle symposium (2007)

[106] D. Mills, Solar Energy, Vol. 76, pp.19–31 (2004)
[107] L. Rybach and M. Mongillo, GRC Transactions, Vol. 30, 2006

[109] D.C.Grahame, Chemical Review, Vol. 41(3), pp.441-501, (1947)

[110] M. Kruk, M. Jaroniec, and J. Choma, Carbon, V 36, No. 10, pp.1447-1458 (1998)